Volume 7
Number 2
February 2020
Pages 303–626

Materials Horizons

rsc.li/materials-horizons

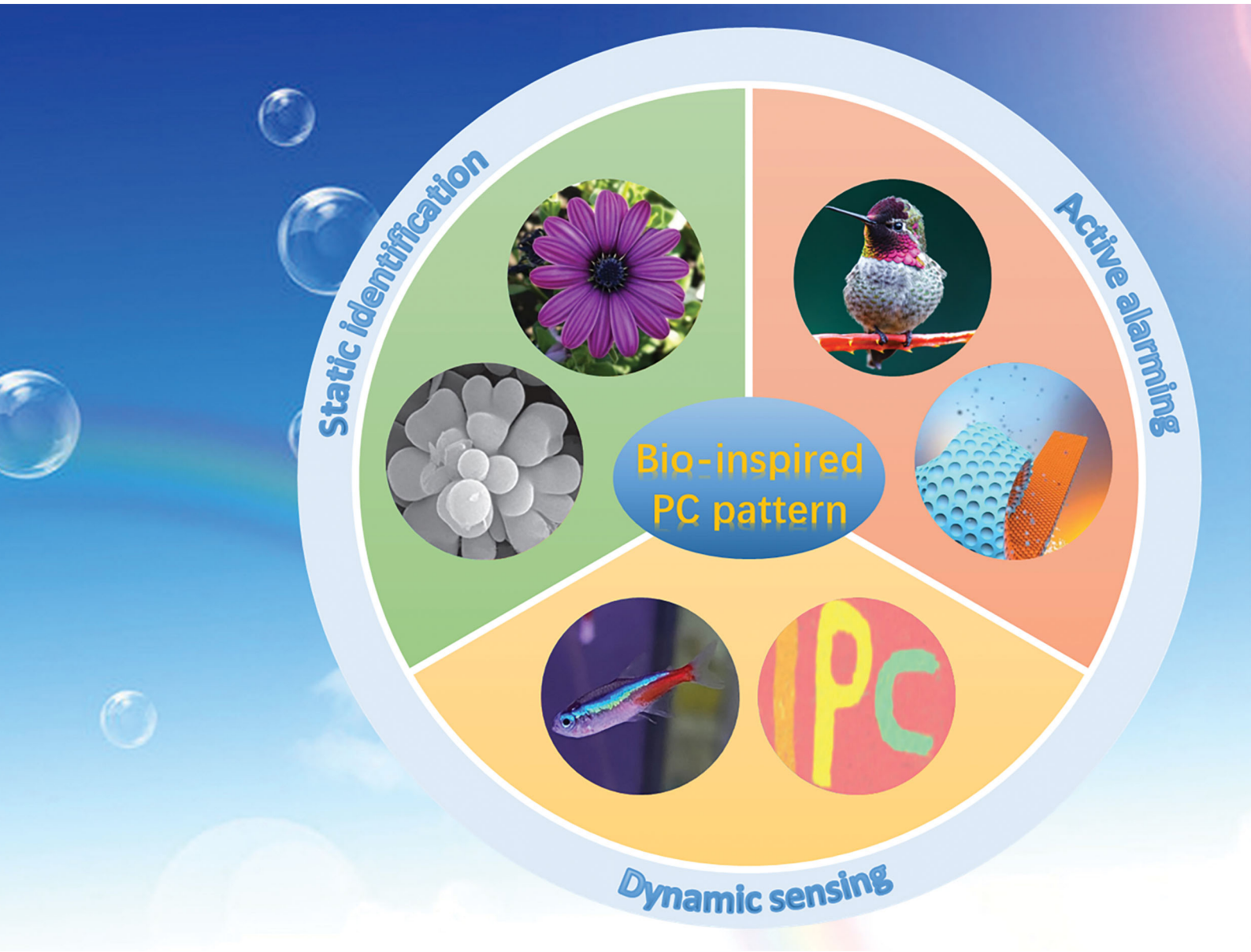

ISSN 2051-6347

ROYAL SOCIETY OF CHEMISTRY

REVIEW ARTICLE
Jingxia Wang *et al.*
Bio-inspired photonic crystal patterns

Materials Horizons

ROYAL SOCIETY OF CHEMISTRY

REVIEW

View Article Online
View Journal | View Issue

Cite this: *Mater. Horiz.*, 2020, 7, 338

Bio-inspired photonic crystal patterns

Pingping Wu,[ab] Jingxia Wang *[abc] and Lei Jiang [ab]

Biological photonic crystal (PC) patterns provide unique functionalities for the survival of creatures, such as the static identified patterns of butterfly wings, the mating function of the eye pattern of peacock feathers and the dynamic warning effect of the changing colour of a chameleon upon external stimulus. Inspired by these special functionalities, patterned PCs have been developed and have attracted considerable research interest due to their potential applications in sensors, catalysts, displays, information security and other fields. This review summarizes the preparation strategies, functional evolution and applications of patterned PCs. First, a series of preparation strategies for PC patterns are summarized, including template-induced assembly and direct writing without a template. Subsequently, the research progress in patterned PCs is sorted based on the evolution of their functionality, such as inactive and responsive (reversible, immobilized and programmed) PC patterns. Various applications of patterned PCs are also described in detail, such as sensing devices with a high sensitivity and fast response, PC displays based on external field regulation, information security anti-counterfeiting devices and shape memory intelligent systems. Finally, the outlook and challenges regarding PC patterns are presented. This review provides a significant foundation for the construction of new functional materials based on patterned PCs.

Received 2nd September 2019,
Accepted 19th November 2019

DOI: 10.1039/c9mh01389j

rsc.li/materials-horizons

1 Introduction

Photonic crystals (PCs) have attracted tremendous research interest due to their potential applications in sensors,[1–12] detection,[13–19] displays,[20–28] solar cells[29,30] and other fields.[31–41] PCs comprise a periodic arrangement of materials with different dielectric constants and have unique light manipulation properties.[42,43] These materials are able to prevent the propagation

[a] *CAS Key Laboratory of Bio-inspired Materials and Interfacial Science, Technical Institute of Physics and Chemistry, Chinese Academy of Sciences, Beijing, 100190, China. E-mail: jingxiawang@mail.ipc.ac.cn*
[b] *Center of Materials Science and Optoelectronics Engineering, School of Future Technologies, University of Chinese Academy of Sciences, Beijing 100049, China*
[c] *Guangdong Provincial Key Laboratory of Optical Information Materials and Technology, Guangzhou 510631, China*

Pingping Wu

Pingping Wu received her Master's degree from Lanzhou University in 2018 and is currently a PhD student under the supervision of Prof. Wang at the Technical Institute of Physics and Chemistry (TIPC), the University of the Chinese Academy of Sciences (UCAS). Her research interest is focused on the fabrication and applications of conductive photonic crystals and energy devices.

Jingxia Wang

Jingxia Wang received her PhD degree in Materials Science from Tsinghua University in 2004. She worked as a postdoctoral fellow in Prof. Lei Jiang's group at the Institute of Chemistry, Chinese Academy of Sciences (CAS), between 2004 and 2006. Acting as an associate professor, she then joined Prof. Yanlin Song's group at the Institute of Chemistry, CAS, between 2006 and 2014. In 2014, being a full professor, she moved to the Technical Institute of Physics and Chemistry, CAS. Her research interest is focused on the fabrication and applications of colloidal PCs with superwettability. She has published more than 100 SCI Journal papers in the field.

of specific frequencies (wavelengths or colour) of light in certain directions, resulting in photonic band gaps.[42–44] Therefore, PCs possess vivid structural colours that originate from the Bragg diffraction of visible light owing to their periodic structure.[42–44] PC materials are widespread in natural creatures[45–50] such as flowers, birds, insects and fish; specific examples include the *red rose petal* and *white hibiscus trigonum petal*.[45,46] The fruit of *pollia condensate* has a multilayer-based strong iridescent coloration, which is attractive for some birds.[50] *Anas platyrhynchos drakes* have iridescent neck feathers.[46] The butterfly has a colourful surface with various patterns.[51] The fresh water fish *neon tetra* can change the structural colour of its lateral stripe from blue-green to indigo in response to light, and change from a light-adapted state to a dark-adapted state.[52] These vivid colours are all attributed to microscale periodic structures. In nature, there exist iridescent and noniridescent structural colour patterns.[46,51–54] The iridescent structural colour is derived from a well-ordered assembly structure, exhibiting an angle-dependent property that the colour varies with the change of the viewing angle. For example, butterfly wings, neck feathers of *anas platyrhynchos drakes* and natural columnar nacre of abalone shells.[46,47,51] The noniridescent structural colour is derived from a short-range ordered but long-range disordered structure, exhibiting an angle-independent property that the colour does not change with the alteration of the viewing angle.[54] For instance, blue feathers of a *cotinga maynana*, elytra of a *longhorn beetle* and red nose with blue stripes of a *mandrill*.[54] Particularly, the unique structural colour patterns of creatures endow them with an intrinsic functionality, such as the static identified function (Fig. 1A–D),[51–53,55] mating function[55] and a dynamic sensing function of warning or protection from natural enemies (Fig. 1E and G).[56–60] For example, various textures and colourful patterns on the wings of butterfly can be used to identify categories, similar to "ID cards" for the creature (Fig. 1C).[51,61,62] The eye pattern of the peacock tail feather has a mating function with the spouse (Fig. 1B).[55,61] In addition to the static identified function, many bio-PCs have dynamic sensing function that their patterns of body surfaces can produce corresponding colour changes to adapt to the natural environment when encountered with external stimuli. The creatures can show a distinct pattern to gain attention or hide themselves when in situations of courtship, competition and environmental changes, indicating their mood.[56–59] For instance, the elytra of beetles *tmesisternus isabella* can change the structural colour to indicate ambient humidity (Fig. 1E).[59]

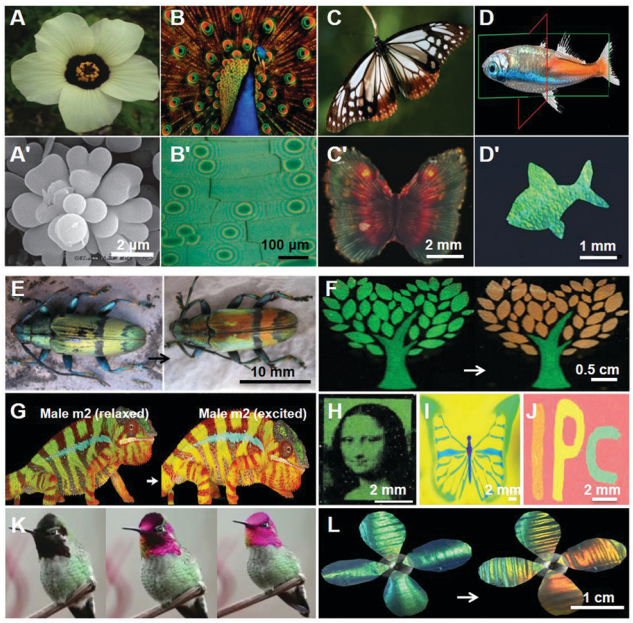

Fig. 1 (A–D) Typical biological PC patterns in nature: *hibiscus trigonum petals* (A),[53] peacock tail feathers (B),[55] a butterfly (C),[51] and a fish (D).[52] (A′–D′) The corresponding artificial PC patterns fabricated in the laboratory: flower-shaped porphyrin Janus particles (A′),[70] an eye pattern (B′),[55] a butterfly-shaped hydrogel material (C′),[66] and a fish-shaped hydrogel material (D′).[66] Reproduced with permission from ref. 53, copyright 2009 The American Association for the Advancement of Science. Reproduced with permission from ref. 55, copyright 2016 Multidisciplinary Digital Publishing Institute. Reproduced with permission from ref. 51, copyright 2009 Springer Nature. Reproduced with permission from ref. 52, copyright 2015 John Wiley and Sons. Reproduced with permission from ref. 70, copyright 2015 Royal Society of Chemistry. Reproduced with permission from ref. 66, copyright 2018 The American Association for the Advancement of Science. (E) The structural colour change of longhorn beetles *tmesisternus isabella* upon a humidity change.[59] Reproduced with permission from ref. 59, copyright 2009 OSA Publishing. (F) Bio-inspired vapor-responsive colloidal PC patterns acquired by inkjet printing.[67] Reproduced with permission from ref. 67, copyright 2014 American Chemical Society. (G) PC patterns cause an active colour change in chameleons.[56] Reproduced with permission from ref. 56, copyright 2015 Springer Nature. (H–J) Functionalized PC patterns obtained in the laboratory based on the specific response of the material, magnetic field and UV curing (H),[71] water vapor dissolution and UV photodegradation of silk fibroin (I),[73] and direct water-writing/electro-erasing on PEDOT inverse opals (J).[74] Reproduced with permission from ref. 71, copyright 2009 Springer Nature. Reproduced with permission from ref. 73, copyright 2017 John Wiley and Sons. Reproduced with permission from ref. 74, copyright 2019 John Wiley and Sons. (K) A face-changing bird in nature. (L) A chameleon-inspired structural-colour rotating pinwheel.[68] Reproduced with permission from ref. 68, copyright 2019 Elsevier.

Lei Jiang

Lei Jiang is a Professor at the TIPC, Chinese Academy of Sciences, and Beihang University. He is an academician of the Chinese Academy of Sciences, Academy of Sciences for the Developing World, and National Academy of Engineering, USA. He received his Bachelor's and Master's degrees from Jilin University, and PhD from the University of Tokyo. He worked as a post-doctoral fellow with Prof. Akira Fujishima and then as a senior researcher in the Kanagawa Academy of Sciences and Technology with Prof. Kazuhito Hashimoto. In 1999, he joined the Institute of Chemistry, Chinese Academy of Sciences, as part of the Hundred Talents Program. In 2015, he and his group moved to TIPC. His scientific interests focus on bioinspired, smart, multiscale interfacial materials with superwettability.

The feature displays an iridescent golden colour marked with a black band in the middle and an irregular posterior black band in the dry state. The golden-coloured region turns red within a few minutes upon interacting with water. The coloured region of the elytra recovers the golden colour after water evaporates and the elytra returns to the dry state.[59] In addition, the colour and shape of the creature can change responding to the external stimulus. For instance, the chameleon changes its striped pattern within a couple of minutes, and the pattern is fully reversible when encountering a male competitor or a potentially receptive female and environmental stimulus;[56–58] a mature male *panther chameleon* can shift the background colour of its skin from green to yellow or orange, and the blue and red patches on the surface become whitish and brighter (Fig. 1G);[56–58] and face-changing birds can change their colour from black to partial red to full red upon an environmental change, such as encountering an enemy or a danger.

Inspired by these interesting phenomena, scientists have conducted extensive research on both static and dynamic functionalities of PC patterns.[63–65] A wide variety of PC patterns have been manufactured in the laboratory based on four aspects: static identified function, dynamic sensing function, multiple actuating sensors and assembly mode replication. Firstly, variously shaped PC patterns were prepared based on the static identified function of natural creatures.[66–69] For example, Wang *et al.* fabricated flower-shaped porphyrin Janus particles through interfacial assembly combined with a water droplet template (Fig. 1A′)[70] based on the *hibiscus trigonum petals* (Fig. 1A).[53] The authors also fabricated an eye pattern inspired by peacock tail feathers (Fig. 1B)[55] through sandwiching a latex suspension between a superhydrophilic substrate and a hydrophobic one by capillary force and convective force (Fig. 1B′).[55] Gu *et al.* prepared butterfly-shaped (Fig. 1C and C′)[51,66] and fish-shaped (Fig. 1D and D′)[52,66] PCs by taking advantage of the mask method and a hydrogel material. Secondly, a PC pattern with a dynamic sensing function was presented in the laboratory. Typically, Gu *et al.* prepared responsive tree-shaped PC patterns inspired by the environmental responsive behaviour of *tmesisternus isabella* (Fig. 1E)[59] *via* introducing the responsive materials into the PC. The leaf pattern changes its colour while being exposed to special vapours (ethanol) (Fig. 1F).[67] Various PC patterns have also been prepared by introducing magnetism,[71] electricity,[72] light,[73] and solvent[73] responsive materials into PCs. Furthermore, the responsive PC patterns can be permanently preserved through crosslinking, curing or chemical reactions. For example, a "Mona Lisa" image was prepared by combining a magnetic field with UV curing (Fig. 1H).[71] A butterfly pattern was manufactured by water vapor dissolution and UV photodegradation of silk fibroin (Fig. 1I).[73] Recently, a programmed erasable/writable pattern was also obtained by direct water-writing and subsequently electroerasing on poly(3,4-ethylene dioxythiophene) inverse opals (PEDOT-IOs) (Fig. 1J).[74] Thirdly, besides colour change, the shape of the PC pattern can be changed upon external stimulus, achieving advanced sensing and detecting properties toward external signals, e.g., an octopus removes its body colour accompanied by a deformation upon external stimuli, and a face-changing bird can change the colour of its feather accompanied by twisting its head upon an environmental change (Fig. 1K). Various PC actuating sensors have been constructed based on these features. Du *et al.* presented a flower-shaped rotating pinwheel that could sense the environment humidity and show non-fatigued vivid colour alterations and programmable shape transformations inspired by chameleon's effect (Fig. 1L).[68] The assembly mode of the biological PC can be copied for the fabrication of iridescent and noniridescent structural colour PC patterns to meet the requirements of different applications. An iridescent structural colour pattern originates from a well-ordered monodispersed latex assembly.[75–83] A noniridescent structural colour pattern originates from the breakage of a long-range ordered structure and assembly of a short-range ordered structure.[69,84–94] Various processes are used for the preparation of short-range ordered structures for noniridescent structural colour patterns, such as spraying a mixture of two different-sized particles,[95] atomization deposition of a silica nanoparticle dispersion accompanied by an additive, poly(vinyl alcohol) (PVA),[24] and stretching the composite film to form short-range ordered nanovoids in the local strain region.[22] Particularly, adding black matter (such as graphene or cuttlefish ink particles) to the amorphous structure is beneficial for yielding bright, highly saturated and brilliant noniridescent structural colour patterns.[95,96] The structural colour of PC patterns is obtained from assembly of spherical particles or non-spherical particles. The non-spherical particles include phase separation of block polymers,[57,97–127] liquid crystal molecules,[83,128–136] polymers,[137–139] *etc.*[140,141] Patterned PCs provide a novel approach to construct PC devices with unique structures and functions, which have become an important express route for various optical applications such as sensors,[1–12] displays,[20–25] anti-counterfeiting[31–34] and optical devices, *etc.*[35–39]

Herein, we summarize the preparation strategies for PC patterns, PC functional evolution and the corresponding applications. First, the preparation strategies for PC patterns are introduced including template-induced assembly and direct writing without a template. Second, the functional evolution of PC patterns is discussed by introducing inactive and responsive PC patterns, whereby the latter falls into a category of reversible, immobilized or programmed PC patterns. Third, the application of patterned PCs is extended to sensing devices with a high sensitivity and fast response, PC displays based on external field regulation, information security anti-counterfeiting devices and shape memory intelligent systems. Finally, the outlook and challenges regarding PC patterns are put forward. This review provides important insight for the construction of new functional materials based on patterned PCs.

2 Preparation strategies for PC patterns

The preparation approach for PC patterns determines their unique functionality and applications in detection,[13–18] displays,[20–28] anti-counterfeiting,[31–34] *etc.*[36–38] The preparation of PC patterns is mainly divided into template-induced assembly and direct writing without a template, based on the formation of either an iridescent

or a noniridescent PC pattern. Template-induced assembly indicates that the pattern is formed based on the template action, such as general template-induced assembly and sandwich-shaped template-induced assembly.[75–81,142–144] Meanwhile, direct writing indicates that the pattern is directly fabricated without a template, such as inkjet printing, drop-coating and spray-coating.[69,84–92]

2.1 Template-induced assembly

Template-induced assembly is a conventional strategy to obtain PC patterns. The approach refers to the assembly of colloidal particles based on the microstructure substrate. During the assembly process, the microstructure induces the assembly of colloidal particles.[145,146] Specifically, the colloidal suspension dries on a pre-designed microstructure substrate, and the nanoparticles self-assemble into an ordered PC pattern under space constraints and external force interactions.[76,77,147] There are many factors influencing the assembly process and assembly structure, such as the shape, dimension and morphology of the template;[75,148,149] the hydrophilic–hydrophobic properties of the substrate;[77,150] the wetting and dewetting processes;[78,148,151,152] and the environmental condition.[76,147,153,154] Recently, a novel sandwich-shaped assembly system was developed based on the template-induced assembly, *i.e.*, a nanoparticle solution was confined between a chosen flat substrate and a pillar-structured silicon template.[80,81] The assembly of micropatterns with controlled orientation was directly achieved on the flat substrate by solvent evaporation and wetting control. A series of assembly patterns have been obtained based on this method.[155–162]

2.1.1 General template-induced assembly. Template-induced assembly was the earliest fabrication approach for PC patterns and has been greatly developed in recent decades. The research on template-induced assembly involved the formations of simple,[76,164] complicated,[148,149] large-scale[75] and functional patterns[165] in four steps. The template-induced assembly was firstly put forward by Ozin *et al.*, and they prepared PC patterns through capillary force and space constraints.[76] Meanwhile, Xia *et al.* presented complex aggregates of monodispersed colloids with well-defined sizes, shapes and structures through a template-assisted self-assembly.[145,146] During the development process of the assembly, the microstructures of the template are important and determine the resultant assembly pattern based on the combined effect of spatial confinement and an external force induction originated from the template.[75,76] For example, Ozin *et al.* presented a planarized opal-based microphotonic crystal achieved through a direct evaporation-induced assembly, where the shape, size, and orientation could be controlled by space constraints (Fig. 2A).[76] A further study showed that a pattern derived from surface energy (such as a hydrophilic–hydrophobic patterned substrate) could also induce the latex assembly and pattern formation.[77,150] For example, Gu *et al.* fabricated patterned colloidal crystal films based on the distinct wettability of a substrate. The latex particles were assembled on the hydrophilic regions and no assembly developed on the hydrophobic region (Fig. 2B).[77] Recently, special equipment and technologies have been introduced for template-induced assembly to achieve patterned PCs with a controllable thickness,

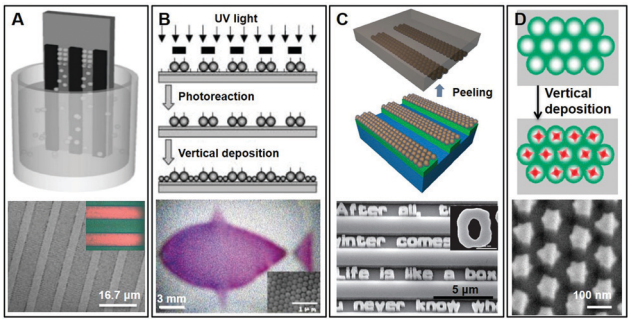

Fig. 2 (A) PC pattern induced by nanoparticle assembly based on space constraints and the capillarity effect.[76] Reproduced with permission from ref. 76, copyright 2002 John Wiley and Sons. (B) The patterning of a colloidal crystal film assembled on a modified hydrophilic and hydrophobic surface.[77] Reproduced with permission from ref. 77, copyright 2002 John Wiley and Sons. (C) Patterned close-packed nanoparticle arrays with controllable dimensions and precise locations.[75] Reproduced with permission from ref. 75, copyright 2012 John Wiley and Sons. (D) The controllable self-assembly of PbS nanostars into ordered structures: close-packed patterned arrays.[163] Reproduced with permission from ref. 163, copyright 2010 American Chemical Society.

area, orientation and morphology; these innovations include layer-by-layer transfer,[149] soft-replicas,[75] microfluidics,[147] printing,[79] *etc.* For instance, Kim *et al.* showed a single monolithic 3D porous silica microstructure with a bimodal pore size distribution that was generated through latex assembly, transfer printing and the thermal decomposition of the binder. Multi-layered porous silica patterns were obtained based on the 3D porous silica microstructure embedded inside an SU-8 microchannel by a site-/shape-selective photolithographic technique.[149] Peng *et al.* fabricated close-packed nanoparticle arrays by combining the synergistic benefits of self-assembly, lithography, and microcontact printing. The ordered nanoparticle arrays were transferred from the air/water interface onto solid substrates with protrusions by using polydimethylsiloxane (PDMS) stamps. A fine control of the overall morphologies as well as the locations of these patterned nanoparticle arrays could be achieved (Fig. 2C).[75] In addition to the technologies and equipment, the assembly of PC patterns has been extended for specific materials. Magnetic nanoparticles were oriented and assembled under the action of a magnetic field, to construct novel PC components.[166] A high-contrast wide-viewing-angle structural colour could be obtained through the assembly of polystyrene (PS) nanoparticles coated with a polypyrrole black coating.[167] More bright and saturated PC patterns were obtained by high-refractive-index materials, such as PbS particles.[163] For example, Qi *et al.* reported close-packed patterned arrays by evaporation-induced assembly routes. Uniform star-shaped PbS nanocrystals (with six symmetric ⟨100⟩-oriented horns) formed highly ordered structures (Fig. 2D).[163] Multicomponent functional particles were demonstrated as well as particles with nontrivial internal structures (such as Janus particles and shape anisotropy particles). These approaches are currently being explored due to their ability to tailor particle interactions and enable the assembly of diverse crystalline structures.[168–172] The structures can be assembled through different interparticle interactions, such as

van der Waals, electrostatic and dipolar.[168] Song *et al.* have conducted a detailed study on the assembly of multi-component functional nanoparticles.[168]

2.1.2 Sandwich-shaped template-induced assembly. Sandwich-shaped assembly was a newly developed approach for the fabrication of PC patterns and was first proposed by Su *et al.* (Fig. 3A).[80,159,160] The sandwich-shaped assembly refers to a nanoparticle solution being confined between a chosen flat substrate and a pillar-structured silicon template, thus, forming a "substrate/nanoparticle suspension/template" assembly system.[80] The microfabricated pillar arrays serve as wetting defects to control the disruption of the nanoparticle solution with solvent evaporation, yielding micrometre-scale liquid bridges between neighbouring micropillars. Such liquid bridges provide a gradually reducing confined space for nanoparticle aggregation; thus, various close-packed assembly patterns can be formed in this special bottom-up way.[155,156,159,160] The sandwich-shaped assembly is based on the differences in the wettability (the surface energy difference between the substrate and the surface microstructure) at the solid interface to control the interface infiltration and dewetting processes, which contribute to large-area, microscale-patterned structures.[80,155,156] The dewetting process is generally affected by these factors, such as the configuration of the silicon template,[80,81] nanoparticle concentration,[81,157] assembly temperature and other parameters.[162] Compared with the general template-induced assembly, the pillar-structured silicon template used in the sandwich-shaped assembly is regular and easily modified for the construction of distinct wettability, which is helpful for the formation of various assembled structures. Importantly, the pattern can be easily transferred onto any substrate during the assembly process. This process was very different from the conventional approach in that the particles were only assembled on the template. Additionally, assembly materials could be extended to a series of functional materials for various applications, such as one-dimensional graphene nanowire arrays for a flexible conductive film and a quantum dot nanowire array for light-emitting diode devices.[160,161] Above all, the sandwich-shaped assembly has clear advantages and great potential for applications in constructing patterned structures.[81,155,161]

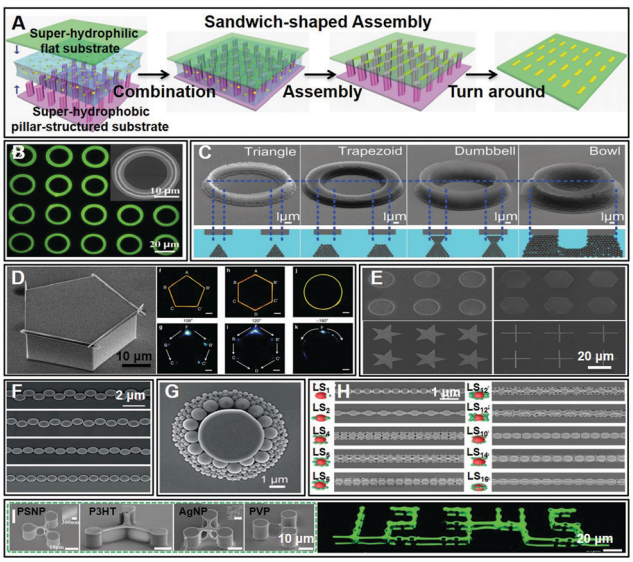

Fig. 3 (A) Schematic illustration of the sandwich-shaped assembly approach.[80] Reproduced with permission from ref. 80, copyright 2014 John Wiley and Sons. (B) A ring-shaped colloidal assembly.[81] Reproduced with permission from ref. 81, copyright 2016 American Chemical Society. (C) The shape-controllable 3D architecture produced by microfluidic engineering of colloidal particles.[162] Reproduced with permission from ref. 162, copyright 2018 John Wiley and Sons. (D) The positioning and joining of organic single-crystalline wires.[161] Reproduced with permission from ref. 161, copyright 2015 Springer Nature. (E) The large-scale, long-range-ordered patterning of nanocrystals *via* capillary-bridge manipulation.[156] Reproduced with permission from ref. 156, copyright 2017 John Wiley and Sons. (F) The precise assembly of particles for zigzag or linear patterns.[157] Reproduced with permission from ref. 157, copyright 2017 John Wiley and Sons. (G) The formation of multi-component size-sorted assembly patterns by tuneable templated dewetting.[78] Reproduced with permission from ref. 78, copyright 2018 John Wiley and Sons. (H) Programmed co-assembly of one-dimensional binary superstructures by liquid soft confinement.[158] Reproduced with permission from ref. 158, copyright 2018 American Chemical Society. (I) A 3D self-shaping strategy for nano-resolution manipulation of multicomponent architectures.[172] Reproduced with permission from ref. 172, copyright 2018 John Wiley and Sons.

The study of sandwich-shaped assemblies has made three important progress towards the preparation of PC patterns such as the modulation of wettability difference between the substrate and pillar-structured silicon template, the addition of various functional materials towards a promising application, and multi-component functional particle systems. First, various patterned arrays can be obtained based on the wettability difference of the substrate and a pillar-structured silicon template. For example, Su *et al.* demonstrated the first alignment of a wide variety of nanoparticles (*e.g.*, metal, metal oxide, semiconductor, and polymer nanoparticles) in one direction on a large scale through the sandwich-shaped assembly system.[80] Wang *et al.* extended the fabrication of well-ordered colloidal patterns such as linear-, mesh-, cyclic-, and multistopband-based arrays by taking advantage of a superhydrophilic flat transfer substrate and a superhydrophobic groove-structured silicon template, whereby circular colloids showed a unique optic-waveguide behaviour (Fig. 3B).[81] Wu *et al.* subsequently reported the 3D architecture engineering of a colloidal assembly by manipulating the microfluid morphology with controllable cross-sections and shapes. The modification of the microfluid morphology was achieved by tuning the physical parameters of the system and the pinning point number. These factors affected the nucleation location, growth rate, architecture orientations and the waveguiding distance (Fig. 3C).[162] Second, the assembly materials can be expanded to various functional materials towards promising applications, such as the assembly of graphene nanowires, quantum dot nanowires, organic single-crystal arrays, nanocrystal superlattices, *etc.* For example, Wu *et al.* reported organic single-crystal wires with fine control over the growth, alignment and the position based on the guidance of pillar-structured substrates by a physical vapor transport technique. The as-prepared highly aligned wires possessed dimensions of a submicrometric width and hundreds of micrometres in length (Fig. 3D).[161] In this process, Wu *et al.* demonstrated a capillary-bridge manipulation method for directing the dewetting of the nanocrystal suspension and achieved long-range-ordered

superlattice structures including lines, circles, squares, pentagons, hexagons, pentagrams, and cross arrays (Fig. 3E).[156] Third, the sandwich-shaped template-induced assembly method can be further expanded for multi-component functional particle systems.[157,158] For instance, zigzag and linear assemblies of isotropic particles were obtained by modulating the viscosity of the system. The programmed co-assembly of 1D superstructures was achieved by liquid soft confinement.[158] Typically, Song *et al.* presented precise control over particle assembly into zigzag and linear patterns (Fig. 3F).[157] The formation of an intermediate assembly state could be controlled by adjusting the size confinement ratio. The evolution from the intermediate state to final assembly structures could be modulated by varying the viscosity of the assembly system. Moreover, the orientation of these assembly structures could be well-controlled for different patterns (Fig. 3F).[157] In this work, they fabricated dual-ring patterns, "comet" structures, and patterns with component separation. The assembly process for particles was well-controlled and different size-sorted assemblies of multiple components were realized by capillary confinement and the templated dewetting effect (Fig. 3G).[78] Furthermore, the authors proposed a programmed co-assembly of 1D binary superstructures by liquid soft confinement. The binary particle assembly was achieved by stepwise confinement and programmed co-assembly in a spatially tuneable liquid soft confinement process. The approach was applicable for various particles of different sizes and materials (Fig. 3H).[158,168] Furthermore, a 3D liquid self-shaping strategy was put forward for rapidly patterning materials over a series of compositions and accurately achieving micro- and nanoscale structures. The pre-designed template offered a pinning region for the droplet, and the surface energy minimization drove the self-shaping process. This process could fabricate micro–nano-geometric patterns without a modelling programme, which would be of great significance for the development of 3D functional devices (Fig. 3I).[172] The sandwich-shaped template-induced assembly provides a new path for further fabrication of PC patterns and the development of new applications for PC-based optic devices.[81,155,161]

2.2 Direct writing without a template

Direct writing has become an important fabrication approach for PC patterns in recent years. Direct writing refers to the process in which pre-designed PC patterns are fabricated by a certain technique or equipment (for example, inkjet printing and spray-coating).[84–90] The pre-designed patterns can be obtained by photolithography, masking or computer output, and the nanoparticles are quickly assembled in the patterned area.[88–91,95,96] Compared with template-induced assembly, direct writing exhibits the advantages of simplicity of the operation process, large-area preparation and cost-effectiveness. Various patterns with noniridescent structural colours can also be obtained by direct writing.[69,85,89–92,95,96] Inkjet printing is the earliest and most frequently used approach, while drop-coating and spray-coating are usually used for the fabrication of noniridescent PC patterns.

2.2.1 Inkjet printing. Inkjet printing has emerged as a particularly attractive patterning technique to accurately deposit small quantities (tens of picolitres) of materials and has been applied in micro-electronics, micro-analysis, micro-fabrication, *etc.*[178] In particular, inkjet printing has been regarded as promising for the achievement of micro-/nanoperiodic structures for next-generation photonic and display devices.[85,88,175,179–184] Inkjet printing refers to inputting the desired pattern or graphic into the computer or drawing the graphic directly with the computer. The characteristic digital signal obtained from the graphic or pattern conversion is transmitted to the printer. The printer controls the printing nozzle system (through an electrical signal) and the ink droplets form the corresponding image on the print carrier.[178] There are many factors influencing the preparation of PC patterns through inkjet printing, such as ink composition,[84,86,88,98,175,177] substrate wettability,[86,87,174,185–188] inkjet printing parameter settings[173,189] and environmental conditions.[190,191] Inkjet printing can directly shape the raw materials without masks or moulds in a cost-effective way. Patterned PCs with different functions have been printed by regulating the composition, solvent and properties of the colloidal particles.[87,88,175,179]

Typically, Song *et al.* have made great contributions to the preparation of functional patterned PCs through inkjet printing technology, and the researchers put forward effective fabrication of dot-,[85] line-,[174] and surface-shaped[87,178] micropatterns with inkjet printing. First, dot-like PC patterns with a regular shape were prepared on a hydrophobic substrate by controlling the sliding of the three-phase contact lines (TCLs) of the substrate (Fig. 4A). The latex particles were well assembled based on the receding TCL. As a result, patterned PC domes with angle-independent structural colours were prepared with a high height-to-diameter (H/D) ratio and close-packed particle assembly. The H/D ratio of the resultant deposition increased with the receding contact angle of the substrate. Owing to the close-packed latex assembly, the as-produced PC domes presented an enhanced fluorescent intensity (more than 40 times) and an excellent wide viewing-angle property (from 0° to 180°). The result provided a simple and efficient strategy to achieve angle-independent structural colour patterns (Fig. 4A).[85] Furthermore, the researchers fabricated various 3D micropatterns (lines, quadrilaterals, stars, hexagons, and octagons) from single droplets by designing a surface energy difference between the hydrophilic patterns and the hydrophobic surface (Fig. 4B). The TCLs forced a droplet containing nanoparticles to be pinned at the patterned hydrophilic points but to be asymmetrically dewetted on the hydrophobic surface (Fig. 4B).[86] Interestingly, 3D microstructures could also be precisely printed on a surface with tuneable dynamic dewetting properties under magnetic guiding *via* the 2D interface manipulation of droplets. By tuning the dynamic dewettability, diverse 3D microstructures including hat-, cone-, pillar-, and spindle-shaped ones were formed (Fig. 4C).[173] Thereby, 3D arrays with accurate positioning and oriented patterns were facilely printed, demonstrating high controllability and the large-scale fabrication of uniform 3D microstructures.[173] Second, a line-shaped PC pattern was prepared by regulating the dynamic aggregated fusion of ink droplets by changing the surface tension of the ink and the concentration of the nanoparticles (Fig. 4D).[174] In this case, controllable footprint lines were printed on substrates

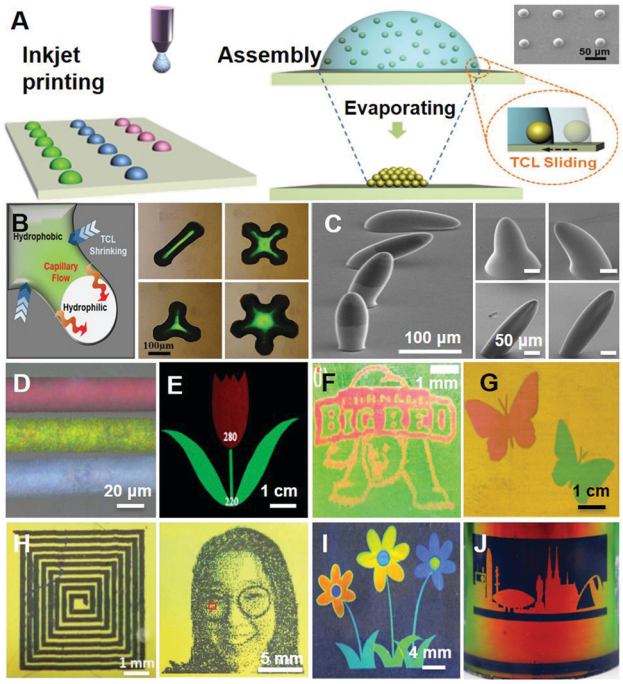

Fig. 4 Inkjet printing approach to obtain PC patterns. (A) Schemes for the inkjet printing of PC dots and domes,[85] (B) complicated 3D micropatterns by inkjet printing combined with a microtemplate,[86] (C) 3D microstructures and arrays from magnetic particles,[173] (D) footprint lines[174] and (E) large-area flower patterns.[87] Reproduced with permission from ref. 85 copyright 2014 John Wiley and Sons. Reproduced with permission from ref. 86, copyright 2015 John Wiley and Sons. Reproduced with permission from ref. 173, copyright 2015 John Wiley and Sons. Reproduced with permission from ref. 174, copyright 2014 American Chemical Society. Reproduced with permission from ref. 87, copyright 2009 Royal Society of Chemistry. (F and G) Directing patterns based on new types of inks such as silicone oils (F)[175] and high-refractive-index CdS spheres (G).[88] Reproduced with permission from ref. 175, copyright 2011 American Chemical Society. Reproduced with permission from ref. 88, copyright 2017 American Chemical Society. (H) An inkjet printing pattern on inverse opals using ethyl acetate as the ink.[176] Reproduced with permission from ref. 176, copyright 2019 John Wiley and Sons. Functional PC patterns were prepared using cholesteric liquid crystals (I)[177] and oxetane liquid crystals (J)[84] as inks. Reproduced with permission from ref. 177, copyright 2018 Royal Society of Chemistry. Reproduced with permission from ref. 84, copyright 2019 American Chemical Society.

based on the coalescence of ink droplets because of their different dynamic wettability properties. As a result, spherical-, line- and dumbbell-shaped patterns were obtained.[174] Third, large-area patterned PCs were obtained by eliminating the coffee ring effect during the inkjet printing process. The coffee ring effect was caused by the uneven deposition of colloidal particles owing to the pinned TLC on a hydrophilic substrate. When the liquid evaporated, the particle mainly deposited towards the brim of the TLC, forming the coffee-ring phenomenon. The elimination of the coffee effect was achieved by adjusting the wettability of the substrate or adding a second solvent (with a high boiling point and low surface tension) to the solution system.[87,178] For example, patterned PCs (red petals and green leaves) with multiple stopbands (Fig. 4E)[87] were fabricated on a hydrophobic substrate by common inkjet printing using polymer latex suspensions as inks. The homogeneous deposition indicated the perfect elimination of the coffee-ring.[87] In addition, Wang *et al.* printed humidity-responsive PC patterns, and a fast response property was induced by the inkjet printing of colloidal PC microdots and the hydrophobic transition of poly(*N*-isopropyl acrylamide) (PNIPAm).[187]

In addition, the printing of functional PC patterns has been developed using new types of ink, such as silicone oil[175] and colloidal particles with a high refractive index.[88] For example, Erickson *et al.* printed erasable, high-resolution colour images using transparent inks on self-assembled PC substrates. The pattern was obtained by infusing a fine drop of silicone oil into the crystal, whereby the oil swelled the structure of the PC and led to a redshift in the stopband. Multicolour images with resolutions of 200 μm were obtained from oils of different molecular weights and the image could be erased by a low vapor pressure oil (Fig. 4F).[175] Furthermore, Wu *et al.* printed large-scale computer-designed butterfly-like PC patterns on photonic paper using high-refractive-index inks containing monodisperse CdS spheres. The inks contained uniform CdS spheres of different diameters but similar intrinsic colours so that the invisible patterns could be observed clearly by simply changing the viewing angle (Fig. 4G).[88] Various functional patterns have also been printed for different applications based on an inverse opal structure and a liquid crystal material with 1D PC characteristics.[84,177] For instance, Omenetto *et al.* fabricated arbitrary PC patterns on inverse opals by using ethyl acetate (as the ink) to locally dissolve PS beads for the designed pattern, followed by aqueous silk solution casting to form a silk/PS composite.[176] Then, a patterned silk inverse opal was obtained by immersing the composite into toluene to remove the PS. In this system, water-soluble biopolymer-based opal structures were used, and a high-resolution image was obtained through the precise deposition of fluids on the PC lattice (Fig. 4H).[176] Schenning *et al.* showed a printable and rewritable photonic polymer coating from a cholesteric liquid crystal. Full colour images could be fabricated with three representative colours (orange, yellow, and bluish green) in the polymer coatings by using the cholesteric liquid crystal as the ink. The printed patterns could be erased by dissolving the E7 ink in tetrahydrofuran, leaving behind a violet coating with no photonic patterns; these erasable coatings could be used as a rewritable paper (Fig. 4I).[177] The authors also fabricated high-resolution PC patterns by using oxetane liquid crystals as the ink. The oxetane-based patterns of iridescent coloured materials have the potential for application both for aesthetic purposes and in anticounterfeiting labels (Fig. 4J).[84]

2.2.2 Drop-coating and spray-coating. Similar to inkjet printing, PC patterns can be fabricated through drop-coating and spray-coating.[69,89–92,95,96] Drop-coating refers to the direct dropping of nanoparticle solutions of different sizes and types onto a specific substrate (or patterned substrate).[89,96] After solvent evaporation, the particles were assembled in a pre-designed area and formed PC patterns. Drop-coating has the advantages of simple operation, low cost and large-area preparation. Spray-coating refers to the latex particles being sprayed by a specific instrument (*e.g.*, a watering can or hand-held spray gun).[90,91,95] Drop-coating and spray-coating are the main ways to prepare

various noniridescent PC patterns. However, there are many factors influencing the preparation of PC patterns through spray- and drop-coating approaches such as the parameter settings of instrument, material composition, substrate wettability and environmental conditions. The formation of a film only takes several minutes, and the process is amenable to large-scale production.[90] Drop- and spray-coating methods enable controlling the pattern for large-area preparation in a simple and cost-effective way.

In a typical drop-coating process, a nanoparticle suspension is dropped onto the substrate, and the nanoparticles are assembled as the solvent evaporates. Various beautiful PC patterns can be obtained by changing the particle size or pattern of the substrate.[89,96] For example, Song *et al.* demonstrated a strategy[89] in which emulsions of monodispersed nanospheres were pre-patterned through direct dropping at a designated position, and a PC pattern with multiple stopbands formed locally within the initial emulsion geometry by simply drying the system on a hot plate. Substrates with wettability patterns were used to fabricate PC designs with complex geometries. By directly dropping the emulsion onto the designated hydrophilic area and then drying rapidly, multi-stopband PC patterns with excellent optical quality and various geometries (such as words, pictures, microfluidic channels, PC tiling and mazes) can be obtained (Fig. 5A and B).[89] Liu *et al.* assembled an amorphous PC structure by drop-coating a mixture of monodisperse PS spheres and cuttlefish ink particles, yielding a noniridescent structural colour.[96] The authors used these artificial structural colours to manifest the logo of ''Fudan University''. Six colours, namely, blue, cyan, green, brown, red, and purple, were obtained by mixing cuttlefish ink particles and latex particles of different sizes (Fig. 5C).[96] A short-range ordered assembly was also realized by spray-coating a mixture of nanoparticles with different sizes, forming large-area angle-independent PC patterns.[90,91,95] For instance, Gu *et al.* sprayed an amorphous colloidal array from self-adhesive poly-dopamine (PDA)-coated SiO_2 nanoparticles. The authors exhibited multi-colour PDA@SiO_2 patterns of the Chinese-style painting of ''Peking Opera'' on glass (Fig. 5E). The bright and noniridescent structural colour of the array was obtained due to the broad-band absorption of PDA. Furthermore, the adhesive forces and fastness of the amorphous colloidal arrays were significantly improved simply by an alkaline vapor treatment (Fig. 5D and E).[90] Zhou *et al.* fabricated highly saturated and brilliant noniridescent structural colour patterns. The short-range-ordered amorphous photonic structures were prepared by introducing graphene nanosheets through a spray-coating process (Fig. 5F).[95] A maple leaf and alphabet letter with vivid red, green, and blue colours were printed on a PVC substrate.[95] Inspired by the common ''milk skin'' phenomenon, Chen *et al.* demonstrated a ''colloid skin''-regulated assembly route for colloidal film deposition that easily suppressed the ubiquitous coffee ring effect accompanying asymmetrical evaporation processes. Combined with either the spray painting or bar coating technique, a large-scale dragon-like pattern was constructed with a uniform morphology, enriched with structural colour and angle-independent spectral properties (Fig. 5G).[91]

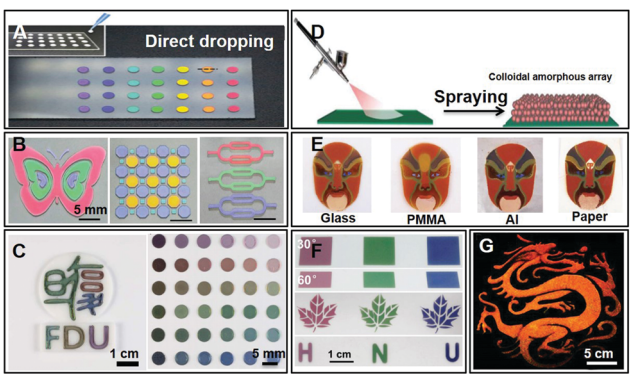

Fig. 5 (A) PC dot arrays with different colours from drop-coating. (B) Butterfly and microfluidic channel patterns were used for information coding, and the security level was further enhanced due to the angle dependence.[89] Reproduced with permission from ref. 89, copyright 2017 Royal Society of Chemistry. (C) The use of cuttlefish ink as an additive to produce noniridescent structural colours of high colour visibility.[96] Reproduced with permission from ref. 96, copyright 2015 John Wiley and Sons. (D and E) Bio-inspired robust noniridescent structural colours with self-adhering amorphous colloidal particle arrays.[90] Reproduced with permission from ref. 90, copyright 2018 Royal Society of Chemistry. (F) Highly brilliant noniridescent structural colours enabled by graphene nanosheets containing graphene quantum dots.[95] Reproduced with permission from ref. 95, copyright 2018 John Wiley and Sons. (G) Large-scale colloidal films with robust structural colours.[91] Reproduced with permission from ref. 91, copyright 2019 Royal Society of Chemistry.

3 Functional evolution of PC patterns

Based on the development of preparation approaches and application requirements, the functionalities of PC patterns experienced an evolution from inactive[75–77] to responsive PC patterns (Fig. 6). Inactive PC patterns are obtained from the assembly of inactive materials, such as PS and SiO_2 particles, block polymers or liquid crystal materials, and they are non-responsive to external stimuli, playing a great role in displays and other fields.[75–77] Responsive patterns are derived from reactive materials,[194–200] and have been developed into reversible, immobilized[71–73] and programmed patterns[201] for various promising applications. In the following part, we mainly describe the research progress in responsive PC patterns. In addition, PC patterns with strain-adaptive stiffness from block polymers are discussed.[103–105,117–119]

3.1 Responsive PC patterns

Responsive PC patterns are obtained by introducing responsive materials into the pattern system, which would respond to external stimuli such as light,[73,202] heat,[193] electricity,[196,203–205] magnetism[206–210] or solvents[194,201] by changing the structural colour and pattern. However, the pattern disappears upon removing the external stimulus,[197,198] therefore, the permanent preservation of PC patterns has been developed by the combination of crosslinked curing and chemical reactions, such as UV-curing,[71,72] infiltration,[211] swelling and metal–organic coordination.[201] Programmed PC patterns refer to patterns that are free of

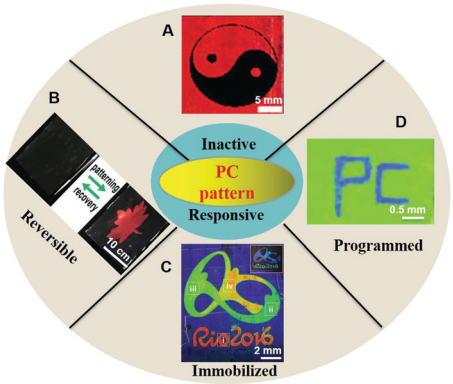

Fig. 6 Functional evolution of PC assemblies consisting of inactive (A)[91] and responsive PC patterns (including reversible (B),[192] immobilized (C),[193] and programmed patterns (D)[74]). Reproduced with permission from ref. 91, copyright 2019 Royal Society of Chemistry. Reproduced with permission from ref. 192, copyright 2019 American Chemical Society. Reproduced with permission from ref. 193, copyright 2016 John Wiley and Sons. Reproduced with permission from ref. 74, copyright 2019 John Wiley and Sons.

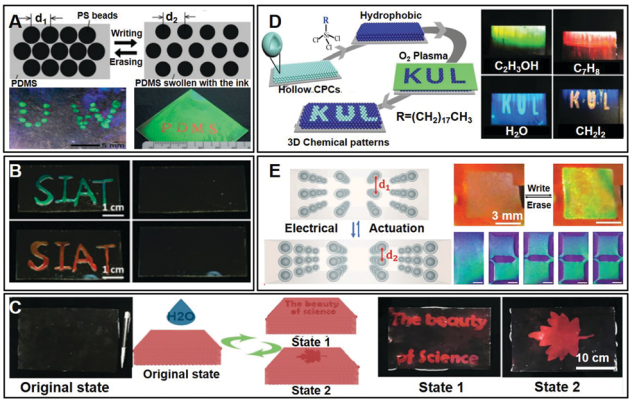

Fig. 7 (A) Photonic papers and inks: colour writing with colourless materials.[195] Reproduced with permission from ref. 195, copyright 2003 John Wiley and Sons. (B) Water as a colourful ink: transparent, rewritable photonic coatings based on colloidal crystals embedded in a chitosan hydrogel.[194] Reproduced with permission from ref. 194, copyright 2015 Royal Society of Chemistry. (C) Large-area and water rewriteable PC films obtained by thermally assisted air–liquid interface self-assembly.[192] Reproduced with permission from ref. 192, copyright 2019 American Chemical Society. (D) A PC pattern induced by the selective interaction between water vapor and hollow SiO_2 spheres.[197] Reproduced with permission from ref. 197, copyright 2018 John Wiley and Sons. (E) Bistable and reconfigurable PC-electroactive shape memory polymer nanocomposites for ink-free rewritable paper.[198] Reproduced with permission from ref. 198, copyright 2018 John Wiley and Sons.

external field stimulation and are erasable as desired. This property is important for the repeatable use of PC substrates and PC patterns.[212,213] Tuneable PC patterns have been widely used in sensors,[67,197] displays[71–73] and anti-counterfeiting.[193]

3.1.1 Reversible PC patterns. The reversible PC pattern is a typical responsive PC, and the pattern can switch upon an external environmental change. Under the action of a specific external field, the lattice structure of the PC pattern changes, which in turn causes an alteration in the structural colour and image, presenting an *in situ* monitoring of the external stimulus, and can be used as an important application in sensors, security labels and displays.[195,197–199] When the external field is removed, the lattice structure and structural colour recover to the initial state, leading to an erasure of the pattern. The formation of reversible PC patterns is mainly due to the swelling/shrinkage effect of a sample towards solvents and the corresponding change in the lattice structure.[194,195,199] For example, Xia *et al.* demonstrated a reversible PC pattern achieved by regional solvent swelling/shrinkage on a colloid-infiltrated PDMS composite membrane (Fig. 7A).[195] As the solvent ink infiltrated into the PDMS network, a swelling of the network and an increase in the lattice spacing led to a redshift in the stop-band and the formation of a PC pattern such as the green-lettered "UV" and red-lettered pattern "PDMS". After liquid ink evaporation, the network returned to its original state and the various letters disappeared (Fig. 7A).[195] Additionally, Wu *et al.* demonstrated a rewritable paper by using water as a trigger to tune the bandgap of the photonic coatings on solid substrates (Fig. 7B). Various colours were achieved by adjusting the particle size of the photonic coatings *via* aqueous solutions of certain pH values. The photonic coatings could be erased and rewritten multiple times without a significant loss in colour quality. Furthermore, the photonic coatings were transparent with good tunability and reproducibility, which allowed for the fast and convenient visualization of the invisible PC patterns with different colours (Fig. 7B).[194] Zhang *et al.* also prepared a water-rewritable PC film as large as A4 size (210×300 mm^2) with a high-quality structure colour (Fig. 7C). The material was obtained by thermally assisted self-assembly at the air–liquid interface. During the assembly process, partially deformed and coalesced nanoparticles appeared with a low glass transition temperature. This process caused the film to be transparent and structurally colourless but still kept the inner 3D-ordered structure. Then, the film could be switched to a structural colour state by interacting with water due to the hydrophilic property of the assembled block. The transition between transparency and structural colour could be reversibly performed multiple times in all or specific regions of the film (Fig. 7C).[192] Clay *et al.* presented the fastest reversible pattern responsive to water vapor (Fig. 7D). The pattern was prepared by introducing invisible patterns (3D chemical patterns) into hollow SiO_2 colloidal PCs (HSCPCs). These hidden images were formed by creating hydrophilic regions (by oxygen plasma etching) in initially hydrophobic HSCPCs (by chemical modification). The result created truly optically invisible patterns under normal conditions, and the visible patterns were obtained with large PC bandgap shifts upon water vapor flow (*e.g.*, human breath), with an ultrafast response of $\approx$100 ms. When the water vapor evaporated, the pattern of "KUL" disappeared, and the system returned to the initial hidden state (Fig. 7D).[197] In addition to the solvents, reversible PC patterns can be achieved by an external field stimulation such as electricity,[72,196,204] magnetism,[71,200,210] photothermal energy,[193,214] *etc.*[196,209] The effect can be attributed to the responsive molecules of the PC system interacting with the external stimulus, causing changes in the lattice parameter and refractive index.[198] For instance, Pei *et al.* developed an ink-free rewritable paper by

combining electroactive and shape memory polymers in a nanocomposite that matched the benefits of paper as a zero-energy, long-term data storage medium, providing additional advantages of rewritability (Fig. 7E). The rewritable paper was made of a Fe_3O_4@C core–shell nanoparticle-based PC embedded in a bistable electroactive polymer. Electrical actuation induced a large deformation in the *z*-axis of the nanocomposite and created a distinct colour change in the actuated area when the temperature of the sample was higher than the melting point. In summary, this nanocomposite stored high-fidelity colour images without inks, the images remained stable for more than a year of storage under ambient conditions, and the stored images could be rewritten over 500 times without degrading. The pattern could be erased and recovered to its initial state by removing the bias voltage and lowering the temperature of the system (Fig. 7E).[198]

3.1.2 Immobilized PC patterns. Reversible PC patterns can be precisely regulated based on the external stimuli (such as a solvent or electric/magnetic field), but the patterns only present under the condition of the specific external field, which limits the extended optical applications of the pattern. Accordingly, it is necessary for the development of effective approaches to immobilize patterns under the condition of external field-action, such as selective immobilization through UV-curing,[71–73] local infiltration[211] and metal–organic coordination.[201] PC patterns are generally regionally fixed, which are beneficial to their precise adjustment and permanent preservation. PC patterns can be regulated by a specific external field depending on the inclusion of magnetic-, electric-, heat- or light-responsive materials.[71–73,201,211] Three approaches were developed for producing immobilized PC patterns, such as photo-[71,72]/heat-curing crosslinking,[193,214] solvent-induced interactions[201] and the combination of multiple effects.[73,202] Immobilized PC patterns have greatly promoted their applications in displays, anti-counterfeiting and other smart materials.[67,71,193]

3.1.2.1 Photo- and heat-immobilized PC patterns. Photo- and heat-crosslinked immobilizations are frequently used approaches for achieving the permanent preservation of PC patterns induced by the external field response. For example, Kwon *et al.* prepared large-area high-resolution PC patterns through magnetic field induction and UV-photocurable regions. The magnetic-ink was a three-phase system consisting of superparamagnetic colloidal nanocrystal clusters coated with a silica-shell, a solvation liquid and a photocurable resin. Under the action of a magnetic field, the superparamagnetic colloidal nanocrystal clusters were assembled to form chain-like structures along the magnetic field lines, where the attractive magnetic force originated from the effect of the superparamagnetic core was balanced by repulsive electrostatic and solvation forces. The combination of attractive and repulsive forces determined the interparticle distance and the corresponding structure colour. Thus, the colour could be tuned by simply varying the interparticle distance *via* magnetic fields. Once the desired colour was obtained, the pattern could be fixed by the photocurable resin upon UV exposure. The chain-like self-assembled colloidal clusters could be frozen in the solidified polymer network by UV photocuring, thus, retaining the structural colour. Accordingly, various patterns (such as trees, triangles, squares, pentagons, circles, and multicoloured bar codes) could be obtained based on this approach (Fig. 8A).[71] Similarly, Ge *et al.* prepared large-area high-resolution PC patterns through electric field induction and UV photocuring (Fig. 8B). The electric-ink was a suspension consisting of single-component colloids, propylene carbonate, supersaturated SiO_2 particles and trimethylolpropane ethoxylate triacrylate (ETPTA). The introduction of propylene carbonate greatly enhanced the response of the colloidal PCs towards the electric field. The presence of ETPTA allowed for the instant fix of the photonic structures and colours. The supersaturated SiO_2 particles spontaneously formed a metastable colloidal PC, which could change the structural colour by assembling/disassembling in a significantly short time. In this system, various patterns, *e.g.*, the petal, stalk, leaves, and stamen of a flower, could be obtained by an electric field with voltages of 0, 3.3, 2.5 and 1.8 V, respectively (Fig. 8B).[72] Li *et al.* prepared a pattern based on the selective photolysis of a photolabile polymer together with the postmodification of released amine groups. The patterning method allowed for regioselective modification within an inverse opal structure by selective chemical reactions (Fig. 8C). The authors prepared a "THU"-shaped pattern consisting of an inert propyl-isocyanate-modified region. The fabricated structure was capable of producing a gradient of photonic

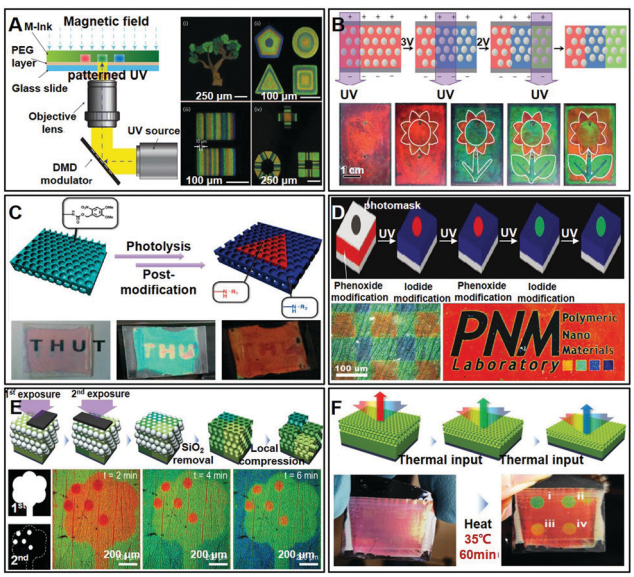

Fig. 8 PC patterns achieved through selective-area immobilization. Patterns induced by a (A) magnetic field and UV curing,[71] (B) electric field and UV curing,[72] (C) selective photolysis modification process,[202] (D) counter-anion with photosensitivity,[97] (E) regioselective thermal compression,[193] and (F) programmed thermal input and compression.[214] Reproduced with permission from ref. 71, copyright 2009 Springer Nature. Reproduced with permission from ref. 72, copyright 2017 John Wiley and Sons. Reproduced with permission from ref. 202, copyright 2015 American Chemical Society. Reproduced with permission from ref. 97, copyright 2012 John Wiley and Sons. Reproduced with permission from ref. 193, copyright 2016 John Wiley and Sons. Reproduced with permission from ref. 214, copyright 2019 John Wiley and Sons.

bandgaps and dynamic chemical patterns based on a self-reporting feature of the PC (Fig. 8C).[202] Kang *et al.* reported a photoresponsive PC gel film with strong reflective multiple colours in the visible region by using polystyrene-*b*-quaternized poly(2-vinyl pyridine) (PS-*b*-QP2VP) block copolymer photonic gels based on counter-anions. The highly swollen photonic gels exhibited large photonic stop band shifts against the weak exposure energy of UV. These findings were useful for understanding the volume transition of polyelectrolyte hydrogels by photo-crosslinking, and were applicable in many fields of science and engineering (Fig. 8D).[97] Heat-curing crosslinking is also an important approach to achieve the permanent preservation of PC patterns. The crosslinking degree can be modified by changing the temperature per curing cross-linking reaction of the photoresist, contributing to the regional PC structure.[193,214] For example, Kim *et al.* designed multicoloured photonic micropatterns through the regioselective thermal compression of inverse opals (made of a negative photoresist); the film shrunk uniformly at high temperatures, resulting in a blueshift in the structural colour, wherein the shrinkage rate was determined by the annealing temperature and the photoresist crosslinking density. A fruit-tree-shaped pattern with green leaves and red apples was presented by combining UV radiation with a mask to produce the multicolour and spatial modulation (Fig. 8E).[193] Kim and Lee *et al.* further designed a PC film that could record the thermal condition *via* an irreversible structural change and intuitive report by colour patterns. The PC films consist of inverse opals made from a negative photoresist on a solid support, whereby the cross-linking density of the photoresist was regioselectively adjusted. The film showed a gradual blueshift in the structural colour upon heating due to anisotropic compression of the inverse opal, in which the stopband shift rate was determined by the temperature and cross-linking density. For a single cross-linking density, the thermal input was quantified from the colour change based on the coupled temperature and time, whereas a multicolour pattern was developed in a single film with multiple cross-linking densities (Fig. 8F).[214]

3.1.2.2 Solvent-induced immobilized PC patterns. Solvent-induced effects have become an important approach to the formation of PC patterns, such as local dissolution, local infiltration and the metal–organic coordination effect. For example, Omenetto *et al.* reported a patterned silk inverse opal by selectively exposing the sample to water vapor or UV light, based on the dual response of silk to water/light (Fig. 9A). A strong interaction between the silk proteins and water molecules took place. This interaction would lead to beta-sheet formation or material dissolution when the system was exposed to water vapor or immersed in water. The deep-UV light was able to induce peptide chain scission and the photodegradation of the silk fibroin at the weaker C–N bonds, leading to the molecular rearrangement of silk fibroin and the pattern fabrication. The authors prepared a flower-shaped pattern using three different stencils and a butterfly-shaped pattern by exposing each image to UV light for different times (Fig. 9A).[73] Aizenberg *et al.* prepared a pattern based on the distinct wettability that was designed by selectively exposing the film to an oxygen

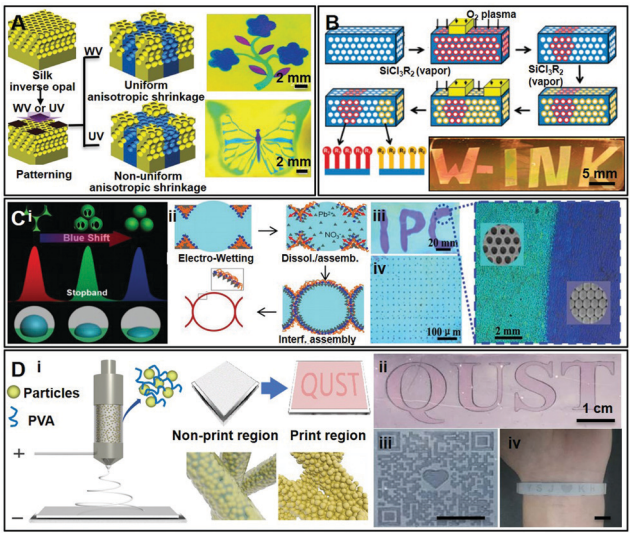

Fig. 9 (A) Painting silk inverse opals with water and light.[73] Reproduced with permission from ref. 73, copyright 2017 John Wiley and Sons. (B) Encoding complex wettability patterns in chemically functionalized 3D PCs.[211] Reproduced with permission from ref. 211, copyright 2011 American Chemical Society. (C) The electrowetting-induced morphological evolution of metal–organic inverse opals towards a water-lithography approach.[201] Reproduced with permission from ref. 201, copyright 2017 John Wiley and Sons. (D) The direct writing of structure-colour patterns on electrospun colloidal fibres towards wearable materials.[212] Reproduced with permission from ref. 212, copyright 2019 Springer Nature.

plasma (Fig. 9B). The researchers used highly ordered 3D PC as a regionally functionalized porous carrier, and the wettability difference was obtained through exposing the entire film to alkyl chlorosilane vapours, followed by a selective exposure to an oxygen plasma. Immersion of the sample in a particular fluid induced the localized infiltration and the disappearance of the bright colour, which led to a larger change in the effective refractive indices between the wetting and non-wetting regions, contributing to the formation of a pattern (W-INK) with an encoded complex wettability (Fig. 9B).[211] Wang *et al.* showed a special PC pattern induced by a water-lithography approach, *i.e.*, an electrowetting-induced morphological evolution on a metal–organic inverse opal (Fig. 9C). The morphology of the building blocks changed from interconnected pores to separated hollow spheres during the electrowetting process, which was accompanied by an unusual blueshift in the stopband position and by the decreased wettability of the film. This morphology evolution was attributed to the simultaneous collapse/reconstruction of the metal–organic frame owing to the partial dissolution of the metal salt ($PbNO_3$) and to the interface assembly of the metal–organic coordination around the skeleton (Fig. $9C_{i,ii}$). The adjustable morphology could be developed as a novel and simple water-lithography approach for the creation of PC patterns. For example, an irreversible "IPC" pattern was fabricated by simply dropping a water droplet to trace the pattern "IPC" on the surface, which resulted in a colour change from green to cyan (Fig. $9C_{iii,iv}$).[201] Recently, the authors also presented direct-writing structure-colour patterns on electrospun colloidal fibres by inkjet printing (Fig. 9D). The pattern formation was attributed to the morphological

transition of the colloidal fibre from fibre aggregation to latex aggregation and the corresponding colour changed due to the dissolution of PVA by water. A non-distinct and blurred image was obtained from the direct printing of water onto the super-hydrophilic pristine film, while a clear and clean image was successfully printed onto the less-hydrophilic colloidal fibre treated with ethanol (Fig. 9D$_i$). The ethanol treatment could compact the fibre structure by lowering the spreading/wetting behaviour of the ink on the fibre structure, which contributed to the formation of high-quality patterns. For example, various letters and two-dimensional codes were flexibly designed and printed on colloidal fibres (Fig. 9D$_{ii,iii}$), and the patterns could be easily transferred onto a flexible substrate, *i.e.*, a flexible printed bracelet (Fig. 9D$_{iv}$).[212]

3.1.2.3 Solvent- and stress-immobilized PC patterns. Recently, a new approach for PC pattern formation was demonstrated and was based on the combined effects of solvent and stress on a polymer. By this approach, Sivaniah and Ito *et al.* prepared the world's smallest "Kanagawa Surf" image without using any paint (a width of only 1 mm). The researchers managed to control the formation and organization of microcavities and microfibres by the stress crazing of polymer films, producing structural colours throughout the visible spectrum. The "organized stress microfibrillation" technique consisted of two points: a weak solvent and a standing wave. The weak solvent referred to the solvent being generally too weak to dissolve the polymer but being capable of penetrating and plasticizing the polymer to accelerate the formation of microcavities and microfibres, thereby accelerating stress cracking. The standing wave referred to the formation of a controlled and organized stress field within a polymer film to induce stress cracking. A multi-layered porous microfibrillated structure was formed in a polymer film by combining the weak solvent and standing wave, exhibiting full visible-spectrum structural colours (Fig. 10A). The structure of the porous microfibre layer was closely related to the type of solvent selected, the temperature and the wetting time. The colour of the film could be adjusted by changing the preparation method. The researchers used a standard lithography technique to apply a texturized stress microfibrillated process to inkless colour printing (Fig. 10B–G). Resolutions of up to 14 000 dots per inch could be achieved by using micro-LED illumination. Multiple colour images could be created within the same film by applying a different mask for each wavelength (Fig. 10B). The authors also fabricated the "US Airforce Resolution chart" (Fig. 10C and D), a "teenage avatar" (Fig. 10E) and the "Mona Lisa" painting (Fig. 10F and G) *via* micro-LED illumination and a solvent.[215] The as-prepared film exhibited a porous network structure, and it is breathable and suitable for wear. The material could be used in medical and health fields, e.g., to provide the necessary biomedical information to healthcare personnel with the skin surface. The development of this technology was expected to remove the dependence of colour printing on pigments.

3.1.3 Programmed PC patterns. Although the desired PC pattern can be preserved by UV/heat crosslinking and other methods, the solidified image was only maintained and could not be removed for the special requirement. Therefore, challenges remain in the development of novel PC patterns that are free of external fields and are erasable as desired. This property is important for the repeatable use of PC substrates and PC patterns, and provides certain prospects for the creation of novel PC paper and e-paper. For example, Wang *et al.* presented a reversible direct water-writing/electroerasing pattern on PEDOT-IOs (Fig. 11A). PEDOT-IO-0 was fabricated by the potentiostatic polymerization of 3,4-ethylene dioxythiophene such that PEDOT infiltrated the interstices of a PC template, and subsequently, the template was removed. The PEDOT-IO-I was obtained by reducing PEDOT-IO-0 by an electrochemical process. There were specific different switches for PEDOT-IOs (Fig. 11A): one was the reversible electrochemical process between neutral and oxidized PEDOT-IO-I, which was accompanied by a reversible stopband shift owing to ionic doping/dedoping. Another switch was the water-induced removal of ions to enable the transition from PEDOT-IO-I (oxidation state) to PEDOT-IO-II, which induced a blueshift in the stopband (Fig. 11A$_i$). Combining the switches of PEDOT-IO-I and PEDOT-IO-II, a reversible water-writing/electro-erasing procedure was realized in the full-solid state, producing multi-colour patterns by water (a friendly ink) writing for different times. The as-prepared PC pattern could be erased electrochemically (Fig. 11A$_{ii}$). Thus, an erasable e-paper could be successfully achieved based on the switches of PEDOT-IOs, providing a novel method for the fabrication of functional optic materials (Fig. 11A$_{iv}$). Meanwhile, diverse PC patterns could also be prepared by inkjet printing (Fig. 11A$_{iii}$).[74] Similarly, Zhang *et al.* prepared a shape memory PC responsive to near-infrared lasers with high optical reversibility and excellent stability (Fig. 11B).

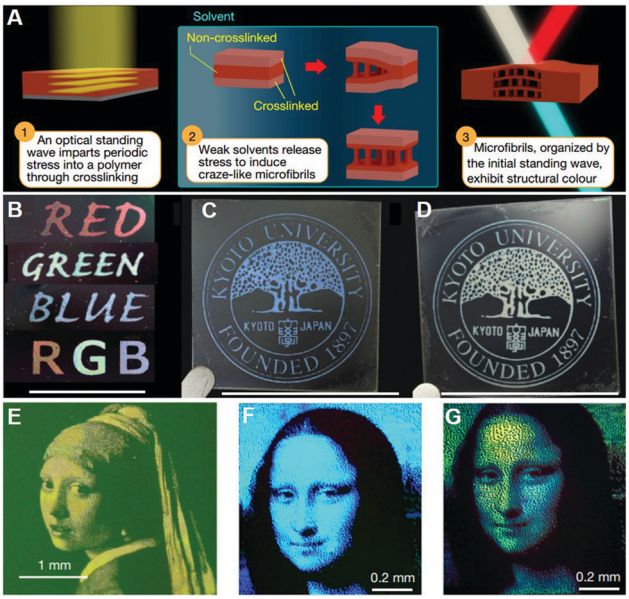

Fig. 10 Structural colour obtained using organized microfibrillation in glassy polymer films.[215] (A) Schematic illustration of PC patterning by solvent and stress. (B) A multicolour image and (C–G) various high-resolution images. US Airforce Resolution chart (C and D), teenage avatar (E), and the Mona Lisa painting (F and G). Reproduced with permission from ref. 215, copyright 2019 Springer Nature.

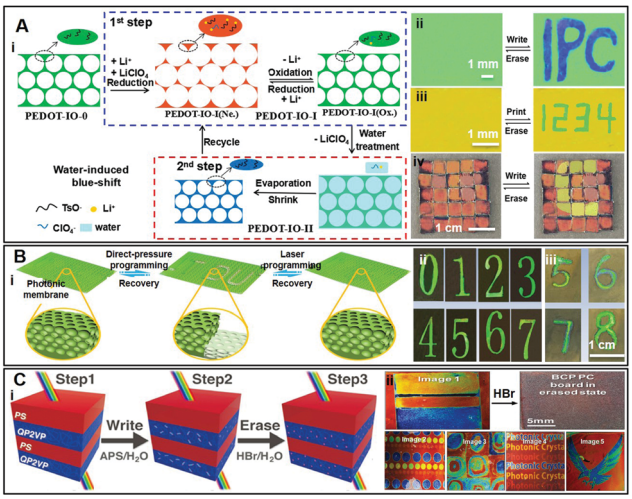

Fig. 11 (A) Direct water-writing/electroerasing of a pattern on PEDOT inverse opals.[74] Reproduced with permission from ref. 74, copyright 2019 John Wiley and Sons. (B) Two-way rewritable and stable photonic patterns enabled by shape memory photonic crystals responsive to near-infrared laser light.[213] Reproduced with permission from ref. 213, copyright 2019 Royal Society of Chemistry. (C) Printable and rewritable full block copolymer structural colour.[102] Reproduced with permission from ref. 102, copyright 2012 John Wiley and Sons.

These shape memory PCs exhibited direct-pressure-induced programming and near-infrared laser (980 nm)-triggered recovery capabilities due to the reversible plastic deformation and the photothermal effect of the polyurethane units (Fig. 11B$_i$). Various rewritable and stable PC patterns could be created by imprinting lithography and near-infrared laser writing. Particularly, a PC membrane exhibited the two-way rewritable capability of imprinting lithography/plastic deformation and laser writing/photothermal effect erasing, through which the programmed photonic patterns could be created twice in one write/erase cycle (Fig. 11B$_{ii,iii}$).[213] Thomas *et al.* demonstrated an inkjet printable and rewritable block copolymer structural colour display, which could be quickly written and erased over 50 times. The writing process used a modified printer with a water-based ink containing a reversible crosslinking agent. The pattern was formed by deposition of the ink onto a self-assembled block copolymer PC film comprising a 1D stack of alternating layers, which caused differential swelling of the written block copolymer film, producing a full-coloured display of characters and images (Fig. 11C$_i$). Furthermore, the information could be readily erased and the system could be reset by application of hydrogen bromide. Subsequently, new information could be rewritten, resulting in a chemically rewritable structural colour display (Fig. 11C$_{ii}$).[102]

3.2 PC patterns with strain-adaptive stiffness

Despite the versatility of synthetic chemistry, certain combination of mechanical softness, strength, and toughness can be difficult to achieve in a single material.[216] These combinations are common in biological tissue, such as chameleons, cephalopods and amphibians. Particularly, active camouflage is widely recognized as a soft-tissue feature, and yet the ability to integrate adaptive coloration and tissue-like mechanical properties into synthetic materials remains elusive; this problem can be effectively resolved by the self-assembly of linear–bottlebrush–linear triblock copolymers.[57] The assembly of block copolymers in the condensed matter state allows access to a range of highly ordered materials with unique nanostructure symmetries and photonic properties, which impart great flexibility to control their chemical and physical functionalities.[112] Typically, a highly reflective polymer film was synthesized from blending of linear homopolymers with brush block copolymers by Grubbs *et al.*[112] Adding homopolymers to the brush block copolymers could improve the overall ordering (or optical properties) and incorporate various functional groups into the films (Fig. 12A).[105] Recently, inspired by the periodic or quasi-periodic structures of the male panther chameleon changing from a relaxed to an excited state, Keith *et al.* prepared chromophoric elastomers that mimicked the characteristics of human skin tissue based on the self-assembly of linear–bottlebrush–linear triblock copolymers.[124] The as-prepared elastomers enabled replication of the mechanical response of strongly strain-stiffening tissues, and mimicked skin tissue—soft on touch, stiff upon deformation, and coloured for appeal or camouflage. The softness and strain stiffening could be enhanced simultaneously by employing a brushlike architecture in solvent-free elastomers. There was a dual mechanical effect between the side chains and network strands. Moduli were reduced to 100 Pa *via* chain disentanglement, and strain stiffening increased *via* strand extension due to side-chain steric repulsion. Microphase separation of the architecturally distinct blocks resulted in physically

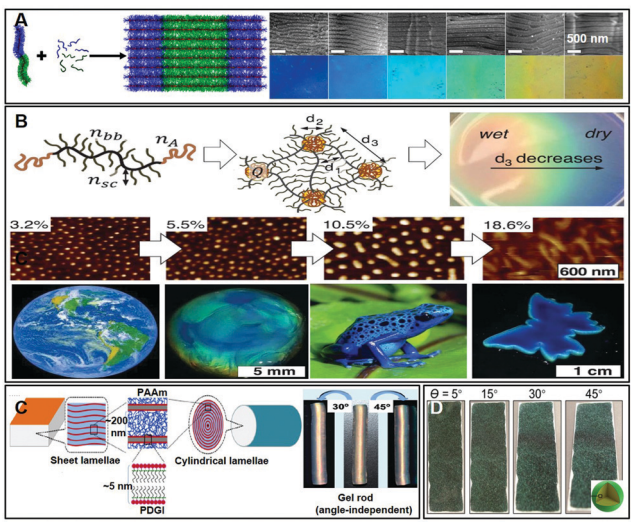

Fig. 12 (A) 1D PC from brush polymers.[105] Reproduced with permission from ref. 105, copyright 2014 American Chemical Society. (B) Chameleon-like elastomers with molecularly encoded strain-adaptive stiffening and coloration.[57] Reproduced with permission from ref. 57, copyright 2018 The American Association for the Advancement of Science. (C) Tough photonic hydrogel displaying programmable angle-independent colours.[124] Reproduced with permission from ref. 124, copyright 2018 American Chemical Society. (D) Hierarchical photonic pigments with angle-independent colours from bottlebrush block copolymers.[114] Reproduced with permission from ref. 114, copyright 2019 American Chemical Society.

cross-linked networks that displayed vibrant colours (satellite image of the Earth and butterfly), extreme softness, and intense strain stiffening on a par with that of skin tissue (Fig. 12B).[57] Additionally, the film assembled from the block polymer showed an amorphous structure and produced non-iridescent structural colour. Typically, composite hydrogels with strong mechanical performances showed angle-dependent and angle-independent structural colours based on the alteration of bulk and internal geometries. The photonic gel sheet exhibited strong angle-dependent colours when the lamellae were aligned parallel to the sheet surface. But the gel rod exhibited an angle-independent colour when lamellae were coaxially aligned in a cylindrical geometry (Fig. 12C).[124] Hierarchical photonic pigments could be achieved *via* the confined self-assembly of bottlebrush block copolymers within emulsified microdroplets by Song *et al.* The bottlebrush block copolymer self-assembled into highly ordered concentric lamellae, giving rise to a near perfect photonic multilayer in the solid state. The concentric lamellar structure (in contrast to a planar geometry) provided a uniform green colour under diffuse illumination (Fig. 12D),[114] with no evident iridescence. But the film exhibited strong iridescence with a blueshift observed at large angles ($\Theta > 30^{\circ}$) under direct illumination.

4 Applications of patterned PCs

Compared with PCs, patterned PCs provide incomparable functions for their potential applications. PC patterns present particular express way that is more vivid than structural colour of PCs. The specific pattern can be well designed to identify the targeted application environment, for example, the pattern can be designed as an image, letter, special logo, or even moving movie, indicating the signal, action, mood, *etc.*, which is far more complicated than just 7 kinds of structural colour. Therefore, patterned PCs have been widely used for the rapid detection of ions,[15,217,218] gases,[1,219,220] biomolecules[3,4,13,16,17,221,222] and other materials,[223–225] demonstrating the potential for applications in sensors,[1–8] displays,[20–25] information security[31–34] and shape memory systems.[35–38] These colourful display devices and anti-counterfeiting patterns mainly depend on the unique structural colour and specific pattern of the PCs, with the advantages of high brightness, saturation and the absence of fading.[24,25,31–33] Moreover, the combination of PC patterns and shape memory polymers provides unique functionalities for new intelligent systems.[36–38]

4.1 Sensors

Patterned PCs have important applications in sensors due to their unique optical properties and a designable and distinct optical signal responsive to external stimuli. PC sensors mainly include chrominance sensors,[2,220,226–233] fluorescent sensors[13–19,234–236] and actuating-type sensors[5–8,237–242] based on their intrinsic properties. In a chrominance sensor its structure colour can respond to an external stimulus,[2,228,229] while the fluorescent sensor allows for a fluorescent signal to be magnified by the PC structure and used for detection.[16–18,243] For the newly developed actuating-type sensor, its shape/structure colour change is accompanied by an external stimulus.[7,8] These PC sensors greatly extend their applications in various fields.

4.1.1 Chrominance sensors. The intrinsic structural colour of a PC pattern is derived from the Bragg scattering of its periodic dielectric structure. The pattern colour varies according to the changes in structure periodicity and dielectric constant under an external stimulus and provides a simple sensing method by the naked eye. These patterns can be used to detect various environmental stimuli such as forces,[2,9,231] magneticity,[209,220] electricity,[196,203] molecules,[13,16] ions,[15,217,218] and humidity.[1,219] For example, Gu *et al.* reported ethanol vapor sensing based on a tree-like responsive colloidal PC that was fabricated by inkjet printing a mesoporous colloidal nanoparticle ink on substrates. In this system, tree-like patterns showed vapor responsive colour shifts or vapor-revealed images by adjusting the nanoparticle size and the proportion of mesopores (Fig. 13A).[67] Wang *et al.* fabricated a dragon-like humidity sensor *via* inkjet printing of PC microdots. The authors reported a fast response to water vapor of *ca.* 1.2 s. This rapid response could be attributed to the combined effects of the intrinsic small size of the inkjet microdots and the hydrophobic transition of PNIPAm above its

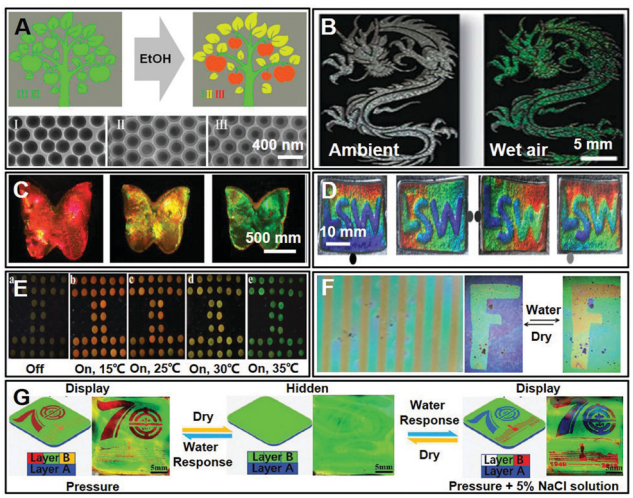

Fig. 13 (A) The pattern PC used for the rapid detection of ethanol vapor.[67] Reproduced with permission from ref. 67, copyright 2014 American Chemical Society. (B) Inkjet-printed colloidal PC microdots with a fast response induced by the hydrophobic transition of PNIPAm.[187] Reproduced with permission from ref. 187, copyright 2012 Royal Society of Chemistry. (C) Colour changes in a bionic butterfly structure colour hydrogel at different temperatures.[223] Reproduced with permission from ref. 223, copyright 2017 American Chemical Society. (D) Mechano-actuated ultrafast full-colour switching in layered photonic hydrogels.[126] Reproduced with permission from ref. 126, copyright 2014 Springer Nature. (E) Rotating 1-D magnetic PC balls with a tuneable lattice constant.[244] Reproduced with permission from ref. 244, copyright 2017 Royal Society of Chemistry. (F) Water-responsive dual-coloured photonic polymer coatings based on cholesteric liquid crystals.[245] Reproduced with permission from ref. 245, copyright 2015 Royal Society of Chemistry. (G) The encoding and decoding of invisible complex information in a dual-response bilayer PC with tunable wettability.[246] Reproduced with permission from ref. 246, copyright 2019 John Wiley and Sons.

lower critical solution temperature. The reversible phase transition of PNIPAm modified the hydrophilic–hydrophobic balance of the polymer interface, which led to the modulation of wetting states/adhesion properties of adsorbed water on the polymer segments. Moreover, the optimal response performance (including signal strength and response sensitivity) of the printed PC microdots was achieved through the synergistic effect of a well-ordered latex assembly and the full infiltration of the responsive polymer in the latex interstices. This simple fabrication of functional colloidal PC microdots opened new avenues for the construction of advanced microanalysis and microsensing devices (Fig. 13B).[187] Zhao *et al.* presented a temperature-responsive PNIPAM-based butterfly-like colour hydrogel, which could shrink/swell *via* different thermal triggers (Fig. 13C). The authors prepared antibacterial structural colour hydrogels by *in situ* integration of silver nanoparticles into the hydrogel materials. The structural colour and reflection peak of the PNIPAM hydrogel gradually blueshift with increasing temperature. Thus, the improved PNIPAm-structured colour hydrogels could be used for detecting temperature changes (Fig. 13C).[223] Gong *et al.* reported a mechano-actuated soft photonic hydrogel with an ultrafast-response time, full-colour tunable range and high spatial resolution, which could be actuated by a very small compressive stress. The photonic hydrogel consisted of uniaxially aligned bilayers and a chemically crosslinked hydrogel matrix, exhibiting excellent mechanical stability. This material could be used in optical devices, such as full-colour displays and sensors to visualize the time evolution of complicated stress/strain fields (Fig. 13D).[126] Guan *et al.* developed 1-D magnetic PNIPAm hydrogel balls with tunable lattice constants. The balls were oriented into periodical 1-D magnetic nanochain-like structures under a magnetic field and UV irradiation. The structural colours of the balls could be regulated by the temperature and solvents. The structural colours could rotate smoothly in the magnetic field direction based on an ''on/off'' switch under various stimuli, and a colourful display was presented with temperatures ranging from 10 °C to 35 °C (Fig. 13E).[244] Schenning *et al.* prepared F-shaped patterned photonic coatings based on cholesteric liquid crystals, which altered their colour when being exposed to water. Various dual-coloured patterns were made, and the patterns were visible in the coating or faded away when placed in water. These effects were reversible and could be repeated several times (Fig. 13F).[245] Zhang *et al.* developed a dual-response bilayer PC to connect the encoding and decoding of invisible complex information (the classic logo for celebrating 70th anniversary of China) by using shape memory polymers with weak hydrophilicity (Fig. 13G). The wettability of the PC was controlled *via* the reversible transformation of the microporous shape of the twisted nanostructures between the spherical and parallel spheres, achieving the structural colour change. Multiple colours were displayed with water penetration into the sample to various degrees, which was derived from the differences in wettability. In addition, the involvement of NaCl in the encoding process could promote water penetration during water exposure, forming a more complicated pattern. These patterns quickly returned to their hidden state after water evaporation. The invisible information could be removed by rewiping with ethanol, achieving the recyclability of the film (Fig. 13G).[246]

4.1.2 Fluorescence sensors. Fluorescent sensors have generally been used for the detection of various external changes (such as ions,[15,218] proteins,[16,236] DNA,[17] glucose, *etc.*[13,14,18,142,234,235]) based on a fluorescent signal. A fluorescent sensor refers to the detection of visible or invisible fluorescent labels by using UV light as the source. The process includes emitting UV light (of a certain wavelength), converting the UV light into visible light and collecting the signal for analysis.[17] PC fluorescence sensors refer to the combination of a fluorescence system and a PC structure, whereby the PC structure can effectively enhance the luminescence based on three aspects: improving the fluorescence efficiency, amplifying the fluorescence signal/detection sensitivity and enhancing the chemiluminescence (CL) intensity/reducing the detection time. First, the PC structure can improve both the fluorescence intensity and fluorescence efficiency.[250–252] The emitted fluorescence exhibits an anisotropic distribution in space owing to the Bragg diffraction effect, and it is possible to selectively enhance the fluorescence signal in a specific detection direction.[15] Therefore, various trace detection and complex system analyses have been developed.[14,18] For instance, Cunningham *et al.* demonstrated an enhancement of the fluorescence emission from colloidal quantum dots coated on the surface of 2D PC slabs, with an enhancement factor of 108 over that of quantum dots on an unpatterned surface (Fig. 14A). The enhancement was due to a combination of high-intensity near fields and strong coherent scattering effects, which could be attributed to leaky eigenmodes of the PC. The enhanced fluorescence was demonstrated by fabricating 2D PC slabs and engineering their leaky modes, where the stopbands overlap the absorption and emission wavelengths of the quantum dots (Fig. 14A).[247] Song *et al.* improved the luminescence properties of a long-lasting phosphor by combining with a PC pattern. The optimized PC structure could double the afterglow intensity and prolong the afterglow time of $SrAl_2O_4$:Eu (a commercially available long-lasting phosphor) by 1.7 times, without any dopants. These results were ascribed to the stopband effect of the PC. The combined PC structure could be beneficial for applications with warning sign shaped long-lasting phosphors in emergency indication, which called for a brighter afterglow intensity and a longer afterglow time (Fig. 14B).[248] Second, the stopband effect of PCs can improve the fluorescence resonance energy transfer (FRET) efficiency, which can greatly amplify the fluorescence signal and the detection sensitivity when the emission peak frequency of the fluorescent molecule matches the stop band of the PC.[17,253] The magnified fluorescent signal can be used for the detection of molecules, ions, DNA and proteins. For example, Song *et al.* prepared an ultra-sensitive DNA sensor by a PC structure containing a fluorescent system (Fig. 14C). The authors improved the FRET efficiency by combining PCs with fluorescence spectroscopy. The fluorescence signal of the acceptor was also enhanced by using a photon-band-gap suppression system, which increased the fluorescence sensitivity of the donor (Fig. 14C).[17] Inspired by the fog collecting structure of the hydrophilic–hydrophobic pattern of

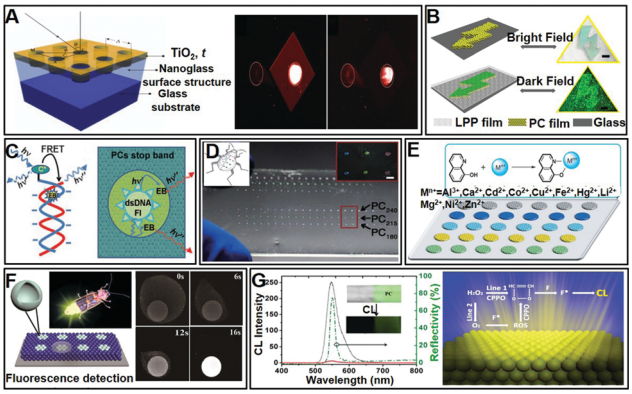

Fig. 14 (A) Enhanced fluorescence emission from quantum dots on a PC surface.[247] Reproduced with permission from ref. 247, copyright 2007 Springer Nature. (B) Efficient luminescent long-lasting phosphor combined with the PC (a warning sign shaped).[248] Reproduced with permission from ref. 248, copyright 2014 American Chemical Society. (C) Ultra-sensitive DNA detection using PCs.[17] Reproduced with permission from ref. 17, copyright 2008 John Wiley and Sons. (D) Bio-inspired PC microchip for fluorescence ultratrace detection.[14] Reproduced with permission from ref. 14, copyright 2014 John Wiley and Sons. (E) A multi-stopband PC microchip for high-performance metal-ion recognition based on fluorescence detection.[15] Reproduced with permission from ref. 15, copyright 2013 John Wiley and Sons. (F) Real-time fluorescence detection in aqueous systems by enhanced photonic surface effects in patterned hollow-sphere colloidal PCs.[18] Reproduced with permission from ref. 18, copyright 2017 American Chemical Society. (G) PC boosted by a chemiluminescence reaction.[249] Reproduced with permission from ref. 249, copyright 2013 John Wiley and Sons.

stenocara beetle's back, Song *et al.* also fabricated a PC microchip with a hydrophilic–hydrophobic micropattern by inkjet printing. This device was used to realize high-sensitivity ultratrace detection of fluorescence signals and fluorophore-based assays, with a detection limit of 10^{-16} mol L^{-1}. This design could be combined with bio-photonic devices for the detection of drugs, diseases, and pollutants of the ecosystem (Fig. 14D).[14] The authors further designed a multi-stopband PC microchip by inkjet printing PC microdots from different latex particles, which could selectively enhance the sensing fluorescence signal in different channels and perform a high-efficiency multi-analyte discriminant test. This PC microchip adopted only one simple sensor of 8-hydroxy-quinoline as the recognition dye for the analysis of 12 metal ions (Fig. 14E).[15] Inspired by the fluorescent worm,[254] Zhong *et al.* realized a real-time ultrasensitive detection approach using hollow-sphere colloidal patterned PCs. This enhancement was mainly due to the band-edge effect of the PC and the wettability differentiation in the superhydrophobic/superhydrophilic pattern. The orthogonal nature of the two strategies allowed for a multiplicative effect, resulting in an increase of two orders of magnitude in the fluorescence signal (Fig. 14F).[18] Third, PCs also enhance the CL intensity and reduce the detection time by increasing CL signals.[249,255] For example, Song *et al.* achieved an enhancement of CL intensity of 44.9 times by introducing a kind of low-cost and feasible artificial PC into a commercial CL system (rubrene-bis(2-carbopentyloxy-3,5,6-trichlorophenyl)oxalate (CPPO)-H_2O_2). It was found that the PC boosted the CL reaction by accelerating the CL decay rate (Fig. 14G).[249]

4.1.3 Actuating-type sensors. In nature, some biological PCs respond to external stimuli by a shape change accompanying their colour change, for example, the octopus is good at both deformation and discoloration upon interacting with external stimuli; the crawling caterpillar and chameleon adjust their skin colours to communicate and create camouflage during locomotion (Fig. 15A).[68,256] Inspired by these features, some novel actuating-type PC sensors have been constructed based on the actuating mechanism.[5–8,237,258–263] An actuator refers to a material that can convert chemical energy into mechanical energy and then undergo a reversible deformation or motion under the stimulation of a certain external field (such as gradient potential of light, electricity, heat, magnetism, solvent, *etc.*).[6–8] A series of PC actuators were developed by combining a PC structure and a responsive material, and the system is capable of responding to

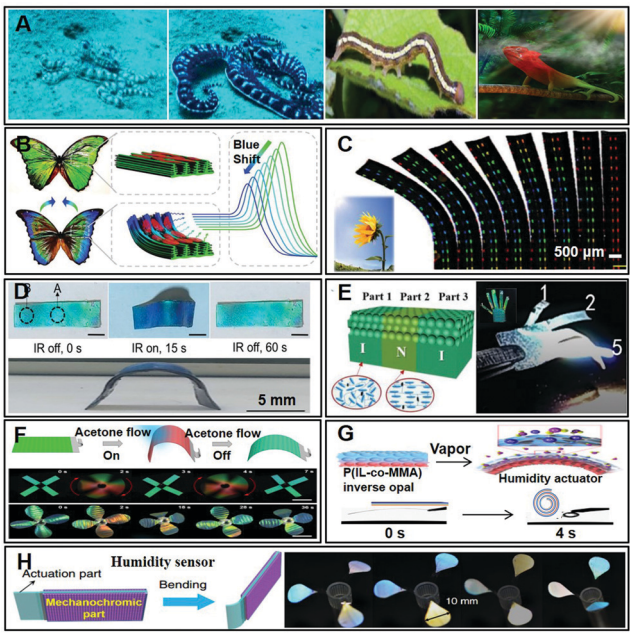

Fig. 15 (A) Deformation and discoloration of an octopus, crawling caterpillar, and chameleon adjusting skin colours to communicate and create a camouflage during locomotion.[68,256] Reproduced with permission from ref. 256, copyright 2018 John Wiley and Sons. (B) Cardiomyocyte-actuated morpho butterfly wings.[8] Reproduced with permission from ref. 8, copyright 2019 John Wiley and Sons. (C) Bioinspired heterogeneous structural colour stripes from capillaries.[6] Reproduced with permission from ref. 6, copyright 2017 John Wiley and Sons. (D) Simultaneous infrared actuation-induced reconfiguration of surface colour and morphology for soft robotics.[257] Reproduced with permission from ref. 257, copyright 2017 Springer Nature. (E) Selective phototriggered actuation and self-oscillation in dual-phase liquid crystal photonic actuators.[258] Reproduced with permission from ref. 258, copyright 2018 John Wiley and Sons. (F) Chameleon-inspired structural-colour actuators.[68] Reproduced with permission from ref. 68, copyright 2019 Elsevier. (G) A hydrophilic/hydrophobic Janus inverse-opal actuator *via* gradient infiltration.[7] Reproduced with permission from ref. 7, copyright 2018 American Chemical Society. (H) A molecular-channel-driven actuator with considerations for multiple configurations and colour switching.[259] Reproduced with permission from ref. 259, copyright 2018 Springer Nature.

the external stimulus by a change in both shape and structural colour, which will greatly improve its sensing and identifying ability. The actuating device can be applied to the biomedicine field. For example, Zhao *et al.* presented a novel cellular-mechanical bio-actuator by assembling engineered cardiac tissues on *morpho butterfly wings* for visible determination. The assembled cardiomyocytes benefited from the periodic parallel nanoridges of the wings and could recover their autonomic beating ability with a good contraction performance. The beating processes caused deformations in the elastic butterfly wing and the corresponding synchronous shift in their structural colours and photonic band-gaps, which served as a self-reporter of the cell mechanics (Fig. 15B).[8] In addition, actuating devices can be prepared for the detection of light signals, such as the near-infrared (NIR), infrared (IR) and UV light. For example, Gu *et al.* prepared an NIR actuator by a strip-like structural-colour material that could be used as an NIR-light-triggered dynamic barcode label for the anti-counterfeiting of different products; the process could mimic the movement of sunflowers that was based on asymmetric light irradiation and a corresponding structural shrinkage (Fig. 15C).[6] Chen *et al.* fabricated a smart film that could change the surface colour and morphology *via* IR actuation (Fig. 15D). The smart film possessed a reconfigurable laminated structure composed of an IR-responsive nanocomposite actuating layer and a mechano-chromic elastomeric PC layer. Upon global or localized IR irradiation, the actuating layer exhibited a fast, large, and reversible strain in the irradiated region, which caused a synergistically coupled change in the shape of the laminated film and the colour of the mechanochromic elastomeric PC layer. Bending/twisting deformations could also be trigged by IR irradiation, which modulated the strain direction in the actuator layer of the laminated film. Such a laminated film was used in a remote-controlled inchworm walker, coupling a colour-changing skin with robotic movements (Fig. 15D).[257] Guo *et al.* developed a phototriggered dual-phase liquid crystal photonic actuator based on 3 parts: the thermal-mechanical component from the liquid crystal polymer, the structural-colour template, and the photothermal-conversion dopant of graphene oxide (Fig. 15E). The dual-responsive liquid crystal photonic actuators were fabricated by photopatterning UV exposure of the nematic/isotropic state, which allowed for selective actuation with versatile actuation modes and complex shape changes. Thus, a phototriggered photoelectric conversion device was constructed by integrating the liquid crystal photonic film with a commercially available poly(vinylidene fluoride) film, that could effectively convert light energy into electrical energy (Fig. 15E).[258] Inspired by the chameleon adjusting its skin colours to communicate and provide camouflage during locomotion, Du *et al.* presented structural-colour actuators that could sense an environmental stimulus and respond with non-fatigued vivid colour alterations and programmable shape transformations (Fig. 15F). These structural-colour actuators exhibited fast colour changes (less than 1 s) and non-fatigued shape transformations (more than 110 cycles), due to their sensitive vaporchromic and robust vapormechanical response properties. The authors further demonstrated applications such as a flower-shaped rotating pinwheel, a closing/blooming flower with brilliant colour changes, and a worm-like walker that could move forward straight and rhythmically with dynamic colour changes (Fig. 15F).[68] Actuating devices can also be prepared for the detection of humidity changes. Wang *et al.* constructed a humidity-responsive strip-like actuating device by introducing an ionic liquid into a PC structure to prepare a hydrophilic/hydrophobic Janus film. The strip-like Janus film demonstrated a directional bending property upon vapor adsorption, and the bending process could be monitored by a spectral change. The Janus characteristics of the fabricated actuator were attributed to the gradient infiltration of the polymer along the film's thickness, which was caused by the gradient light intensity and the distinct polymerization behaviour of ionic liquid and methyl methacrylate in a methanol system. The actuating behaviours were effectively modulated by changing the compositions of the film and the solvent system (Fig. 15G).[7,264] Zhu *et al.* showed a flower-shaped ambient-driven actuator with a rapid response, as well as a self-adaptive and exceptionally stable actuation. The actuator was fabricated through a simple solution processing by taking advantage of inherent nanoscale molecular channels within a commercial perfluoro sulfonic acid ionomer (PFSA) film. The selective patterning of the PFSA film on an inert soft substrate (a polyethylene terephthalate film) facilitated the formation of different movements, including a 2D roll and 3D helical formation in response to water vapor. The chemical modification of the surface allowed the development of a kirigami-inspired single-layer actuator. The actuator was used for detection of personal humidity and heat management based on macroscale geometric design features (Fig. 15H).[259]

4.2 Displays

The bright structural colours of PCs can result in promising materials for next-generation display devices.[20–28] The structural colours produced by PCs have many properties that cannot be mimicked by conventional dyes and pigments. By taking advantage of patterning PCs, novel display devices are to be realized with advantages of low energy consumption, high contrast, and wide viewing-angle property.[207,267–271] The development of PC displays has experienced three stages including electronic, magnetic and liquid crystal displays. The first stage represents electronic-responsive PC displays. The earliest sample was proposed by Ozin *et al.*, who prepared full-colour PC displays based on an electrically actuated reflective flat-panel display technology. The electric field regulated the expansion/contraction of the PC lattice to reflect a narrow wavelength band throughout the visible spectrum.[203] Subsequently, a high-performance electro-active inverse opal gel was prepared consisting of polyferrocenyl-silane derivatives. The film's colour exhibited a continuous voltage-dependent shift (with the Bragg peak scanning the entire visible spectrum) after injecting an electrolyte into the film. But in this case, only the structural colour was improved without the formation of a pattern (Fig. 16A).[196] Electronic display patterns were prepared by Ge *et al.* through sandwiching the ink between two vertical-stripe patterned ITO glass. When UV was irradiated onto the photonic structure to immobilize the pattern, a programmable electrically responsive PC paper cell could be obtained (Fig. 16B).[72] The second stage of PC display involves magnetic-responsive

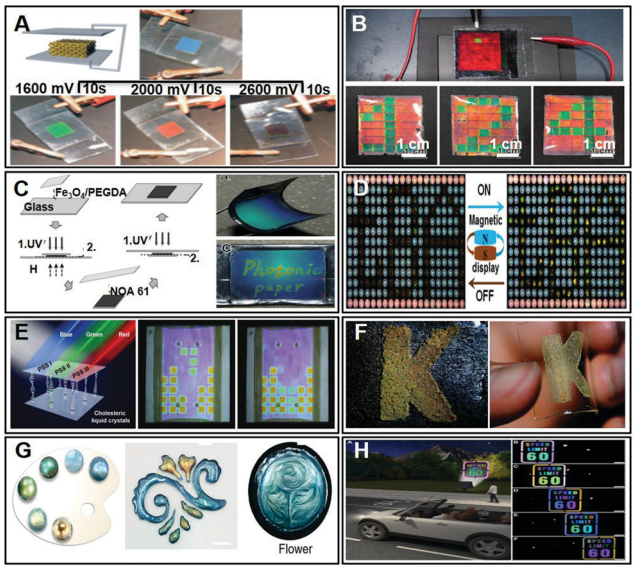

Fig. 16 PC patterns for displays. (A) An all-colour display based on electroactive inverse opals.[196] Reproduced with permission from ref. 196, copyright 2009 John Wiley and Sons. (B) A display device based on electric-field-responsive and photocurable PCs.[72] Reproduced with permission from ref. 72, copyright 2017 John Wiley and Sons. (C) A rewritable PC paper with a hygroscopic salt solution as the ink.[265] Reproduced with permission from ref. 265, copyright 2009 John Wiley and Sons. (D) Hydrophobic poly(*tert*-butyl acrylate) PCs for a robust energy-saving performance.[266] Reproduced with permission from ref. 266, copyright 2019 John Wiley and Sons. (E) Photostationary RGB selective reflection from self-organized helical superstructures for continuous photopatterning.[134] Reproduced with permission from ref. 134, copyright 2019 John Wiley and Sons. (F) Reconfigurable PC capsules containing cholesteric liquid crystals with planar alignment.[131] Reproduced with permission from ref. 131, copyright 2015 John Wiley and Sons. (G) Iridescence in nematics: photonic liquid crystals of nanoplates in the absence of long-range periodicity.[83] Reproduced with permission from ref. 83, copyright 2019 National Academy of Sciences. (H) Iridescence-controlled and flexibly tuneable retroreflective structural-colour film for smart displays.[82] Reproduced with permission from ref. 82, copyright 2019 The American Association for the Advancement of Science.

patterned PC displays. The earliest example was developed by Yin *et al.*, who fabricated a PC paper through the rapid magnetic-field-induced self-assembly of Fe_3O_4@SiO_2 colloids and a simultaneous UV-curing process to fix the PC structures inside the poly(ethylene glycol)diacrylate matrix (Fig. 16C). The PC paper could be fabricated on a glass substrate or a flexible plastic substrate, and hygroscopic salt solutions were used as inks to create durable diffraction colours on the paper. The ink marks could be erased by rinsing the paper in water and drying thereafter. The paper/ink system was environmentally friendly, providing advantages such as paper rewritability, low toxicity of the ink and a flexible polymeric matrix (Fig. 16C).[265] Chen *et al.* showed a letter-shaped magnetic-responsive panel display based on magnetic-optic dual-functional Janus supraballs and a microfluidic strategy.[21,267,268,271,272] The researchers fabricated hydrophobic poly(*tert*-butyl acrylate) (PtBA) PCs *via* a facile soap-free emulsion polymerization. They demonstrated enhanced photoluminescence intensity of the CdSe@ZnS quantum dot film in the LCD device based on the unique photonic bandgap of PtBA PCs. Additionally, Janus supraballs with magnetic-optic dual-functionality could be constructed *via* a microfluidic strategy, and the as-prepared PtBA PCs could be applied in magnetic-responsive panel displays (Fig. 16D).[266] The third is liquid crystal-display patterns; in this case, liquid crystal molecules were used for the production of structural colour patterns. For example, Yu *et al.* prepared an optically rewritable display based on light-driven cholesteric liquid crystals. They proposed a tuning mechanism based on a partial photochemical phase transition, achieving continuous patterning of photostationary red, green, and blue colours in a cholesteric liquid crystal system. The relationship between the light stimulus and reflection colour was established. The red, green, and blue colour patterns could be continuously erased and rewritten under light irradiation with different wavelengths. They showed the "Tetris game" according to the programmable modulation of the cholesteric liquid crystal reflection (Fig. 16E).[134] Kim *et al.* fabricated the K-like photonic microcapsules containing cholesteric liquid crystals with planar alignment based on a microfluidic approach. The cholesteric liquid crystal core and the elastomeric solid membrane were separated by using triple-emulsion drops as templates. The cholesteric liquid crystals in microcapsules could retain their planar alignment, rendering the shape and optical properties highly reconfigurable (Fig. 16F).[131] Cheng *et al.* showed non-periodic nematic liquid crystals of nanoplates, which could display structural colours with only a significant orientational order. The authors fabricated a variety of colourful patterns (such as palette, wave, heart-shaped and flower-shaped coffee art) based on the fluidity of the nematic structure. The colloidal dispersion was able to reflect broad-spectrum wavelengths owing to the loose stacking of nematic nanodiscs. The reflection colour could be further enhanced by adding carbon nanoparticles to reduce the background scattering. The vivid colours of the nematic dispersion could be fine-tuned *via* electrostatic forces based on the addition of an electrolyte (Fig. 16G).[83] Recently, Wu *et al.* demonstrated a smart, energy-efficient, and tuneable retroreflective structural-colour material (traffic safety sign pattern) that was especially suitable for night-time traffic safety and advertisement display applications (Fig. 16H). The authors discovered unique structural colours by partially embedding a monolayer of polymer microspheres on the sticky side of transparent tape, spontaneously forming an interferometric structure on the surface of air-cushioned microspheres. The system remained noniridescent under coaxial illumination and viewing conditions but appeared iridescent under noncoaxial illumination and viewing conditions (Fig. 16H). These unique optical properties and the versatile scalable fabrication process provided a strategy for various large-area applications of robust and intelligent structural-colour films, such as smart display screens, anti-counterfeiting labels and artistic decorations (Fig. 16H).[82]

Recently, a novel wide-viewing-angle PC display was put forward based on a noniridescent structural colour. Here, the noniridescent structural colour pattern was developed by a short-range ordered assembly. For example, Takeoka *et al.* reported various coloured aggregates formed by spraying fine, submicrometre-sized spherical silica particles. The microstructure of the aggregate was isotropic

with a short-range order on a length scale comparable to optical wavelengths, and an angle-independent structural-colour resulted from wavelength-specific constructive interference. The colour saturation of these aggregates could be controlled by the incorporation of a small amount of conventional black particles, such as carbon black. A Japanese-style painting (Mount Fuji) could be successfully drawn using this method (Fig. 17A).[273] PC domes with an excellent wide-viewing-angle property were prepared by Song *et al. via* inkjet printing. The result provided a simple and efficient strategy to achieve angle-independent structural colour patterns. Along with the amplified fluorescent intensity, the fluorescent PC domes exhibited an excellent wide viewing angle from 0° to 180° that benefited from a high H/D ratio. This wide-viewing-angle property was confirmed by the consistent strong fluorescence images for a pattern of ''ICCAS''

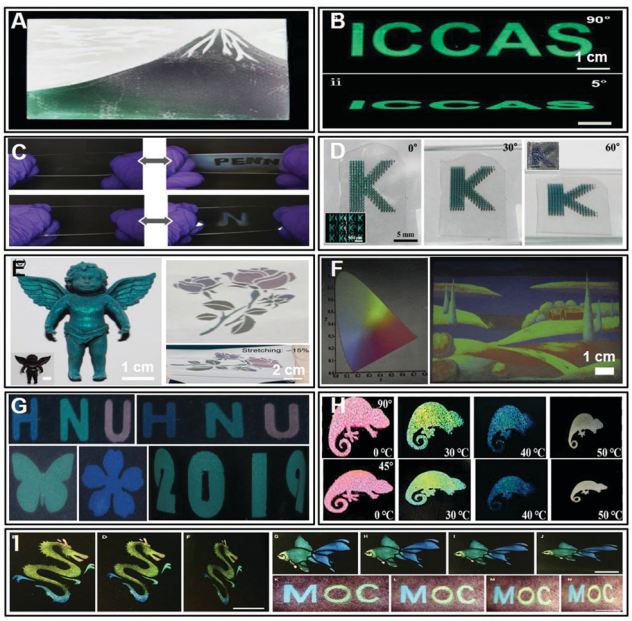

Fig. 17 (A) Production of coloured pigments with amorphous arrays of black and white colloidal particles.[273] Reproduced with permission from ref. 273, copyright 2013 John Wiley and Sons. (B) The inkjet printing of patterned PC domes for wide-viewing-angle displays.[85] Reproduced with permission from ref. 85, copyright 2014 John Wiley and Sons. (C) An angle-independent structural-colour display from stretching of a nanoparticle/PDMS composite film.[22] Reproduced with permission from ref. 22, copyright 2015 John Wiley and Sons. (D) Polymeric inverse glasses for the development of noniridescent structural colors in the full visible range.[93] Reproduced with permission from ref. 93, copyright 2016 American Chemical Society. (E) Noniridescent structural colours with robust mechanical properties fabricated by atomization deposition.[24] Reproduced with permission from ref. 24, copyright 2018 American Chemical Society. (F) Large-scale noniridescent structural-colour printing enabled by infiltration-driven nonequilibrium colloidal assembly.[20] Reproduced with permission from ref. 20, copyright 2018 John Wiley and Sons. (G) Multi-mode structural-colour anti-counterfeiting labels based on physically unclonable amorphous photonic structures with convenient artificial intelligence authentication.[92] Reproduced with permission from ref. 92, copyright 2019 Royal Society of Chemistry. (H) Bio-inspired angle independent structural color films with anisotropic colloidal crystal array domains.[94] Reproduced with permission from ref. 94, copyright 2019 Springer Nature. (I) Bio-inspired self-adhesive bright noniridescent graphene pigments.[69] Reproduced with permission from ref. 69, copyright 2019 Elsevier.

of either the top-view or side-view (Fig. 17B).[85] Yang *et al.* prepared a composite film consisting of a thin layer array of quasi-amorphous silica nanoparticles embedded in the bulk of elastomeric PDMS. The PDMS and silica particle composites were stretched, resulting in the formation of voids around the silica particles. At a certain strain, the stretching process broke the high order of the composite film and caused short-range-ordered nanovoids in the local strain region. Consequently, angle-independent structural-colour displays (PDMS-shaped letters) could be obtained based on such tensile characteristics (Fig. 17C).[22] Kim *et al.* prepared a K-shaped pattern from inverse glasses composed of an amorphous array of air cavities with short-range order (Fig. 17D). They dispersed monodisperse silica particles in a poly(ethylene glycol)dimethacrylate photocurable resin. The particles spontaneously formed the amorphous array with short-range order, which was rapidly captured in polymeric films by photopolymerization of the resin. The inverse glasses displayed structural colours with negligible backscattering in blue due to the short optical path and low index in each cavity. The colours could be tuned in the full visible range by simply controlling the cavity size (Fig. 17D).[93] Zhang *et al.* prepared an amorphous flower-shaped PC pattern with a large area and noniridescent colours by atomization deposition (Fig. 17E). In this case, short-range-ordered amorphous photonic structures were achieved through atomization deposition and solvent evaporation. The as-obtained patterns with a wide viewing angle could be achieved on various rigid and flexible substrates (Fig. 17E).[24] Duan *et al.* fabricated full-spectrum PC patterns (multicolored painting of a landscape) with large-scale and wide viewing angles based on the infiltration-driven nonequilibrium assembly of colloidal particles on liquid-permeable and particle-excluding substrates (Fig. 17F). The amorphous colloidal arrays were obtained within milliseconds (Fig. 17F).[20] Zhou *et al.* fabricated unclonable multi-mode structural colour anti-counterfeiting labels (such as butterfly, flower and letter) based on AI-decodable amorphous photonic structures by introducing an intermediate white layer with water-induced transparency between the patterned amorphous photonic structure layer and the black background layer. The special structural and optical properties of the amorphous photonic structures enabled three-level security functions. The encrypted amorphous photonic structural patterns showed structural colours upon exposure to water, which were conveniently decodable by the naked eye, without any equipment (Fig. 17G).[92] Zhao *et al.* presented a chameleon-shaped structural colour hydrogel by doping spinous pollen particles into colloidal crystal arrays to interfere with their self-assembling process. This material has close-packed anisotropic colloidal crystal domains around the spikes of the pollens. These differently oriented domains could reflect the light to a wide range of viewing angles, contributing to the wide angle of structural colours. The materials showed a light-controlled reversible structural colour change by incorporating photothermal responsive graphene-tagged hydrogels (Fig. 17H).[94] They also presented a graphene-doped noniridescent pigment inspired by mussels' super-adhesivity and feathers' brightness. The elementary unit of the pigments was PDA-adhered multi-shell graphene oxide-encapsulated

silica nanoparticles. These angle-independent patterns (such as Chinese dragon, goldfish, and letters) exhibited higher colour saturation and excellent self-adhesivity properties (Fig. 17I).[69]

4.3 Information security

Anti-counterfeiting techniques have attracted considerable attention because of their widespread application in banknotes, checks, passports, labels, postage stamps and ID cards.[31–34] PCs, as dielectric materials with a periodic modulation for manipulating photons, have demonstrated great success and showed the potential for anti-counterfeiting applications.[272,274–281] In this case, PC patterns were constructed by responsive materials, which could display two or multiple images by changing their colours and transforming between their appearance/disappearance in the background. Patterned PCs provide a new avenue for developing information security devices.[282–289]

Patterned PCs have been extensively studied by scientists for use in anti-counterfeiting labels, information hiding and information storage. For example, Kim *et al.* presented a K-like patterned PC film on a Korean banknote, and the film's colour changed with the incident angle (Fig. 18A). In this system, the colloidal particles were dispersed in a photocurable medium which could infiltrate into a slab by capillary motion. Additionally, the medium permanently solidified the structures *via* photopolymerization. The resultant composite structures exhibited a high transparency or narrow reflection peaks owing to the low-index contrast between the particles and matrix. Therefore, structural-colour mixing could be realized through the overlapping of distinct layers of the colloidal crystals. Multiple narrow peaks in the spectrum provided a high selectivity for optical identification, thereby being potentially useful for security materials (Fig. 18A).[274] Li *et al.* fabricated a four-dimensional screening anti-counterfeiting code composed of differently shaped PC dots that could display four images depending on the lighting condition (Fig. 18B). By controlling the rheology of PDMS, three kinds of PC dots could be sequentially integrated into one pattern using the layer-by-layer printing strategy. The information could be encoded and stored in shapes and read out by measuring the differences in optical properties (Fig. 18B).[34] Zhao *et al.* prepared photonic barcodes for high-throughput bioassays and anti-counterfeiting applications in Fig. 18C. The authors presented an innovative 3D dynamic micromoulding approach for generating photonic barcodes. The dynamic micromould assembly was composed of an immobilized positive microcylindrical-array substrate and a complementarily negative microhole-array mould with flexible positions. Different kinds of structurally coloured microparticles could be assembled with designed sequences or arrays, where the microhole-array mould could be adjusted in the vertical direction. By immersing a pregel solution into the assembled microparticles, photonic barcodes could be achieved through introducing structurally coloured sequences *via* the polymerization of the mixture in the mould holes. The resultant photonic barcodes exhibited a multitude of codes and could be used in high-throughput bioassay and anti-counterfeiting fields. These devices could also be applied in food and pharmaceutical areas by using biocompatible polymers to construct structurally coloured microparticles and photonic barcodes (Fig. 18C).[275] Zhang *et al.* reported a reconfigurable inverse-bilayer heterostructure for PCs, providing a simple and sensitive optical technique for investigating the intriguing encryption effects available at the nanoscale (Fig. 18D). When exposed to ethanol, the anti-counterfeiting code PCs with the inverse-bilayer heterostructure could instantaneously transparentize the top layer and simultaneously release the light reflected from the bottom layer. The transition could quickly return to its original state after ethanol evaporation. Furthermore, the bilayer film showed a redshift in the stopband position upon responsive to water. The mechanism behind the design involved optical scattering and diffraction in the fabricated periodic nanostructures. The effects of scattering and colour superposition of the upper layer could be removed and re-established due to the infiltration and capillary evaporation of fluids with a low surface tension; meanwhile, the system provisionally displayed the pattern of the bottom layer. These characteristics could hide and display information in multiple reversible ways (Fig. 18D).[276] Song *et al.* presented a prototype design for hiding information in PCs by building a coding and

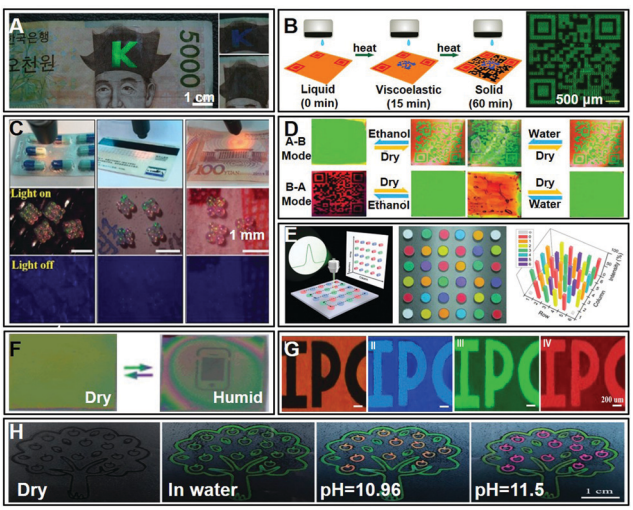

Fig. 18 (A) The patterned PC film on a Korean bank note.[274] Reproduced with permission from ref. 274, copyright 2013 American Chemical Society. (B) Four-dimensional screening of an anti-counterfeiting pattern obtained by inkjet-printed PCs.[34] Reproduced with permission from ref. 34, copyright 2016 John Wiley and Sons. (C) Multicoloured PC barcodes acquired from dynamic micromolding.[275] Reproduced with permission from ref. 275, copyright 2018 Royal Society of Chemistry. (D) A new encryption strategy utilizing PCs with a bilayer inverse heterostructure guided by a transparency response.[276] Reproduced with permission from ref. 276, copyright 2019 John Wiley and Sons. (E) A PC pattern used for information coding, with enhanced security level.[89] Reproduced with permission from ref. 89, copyright 2017 Royal Society of Chemistry. (F) Humidity-triggered photopatternable nanolayered polymeric films with a fast tuneable colour response.[277] Reproduced with permission from ref. 277, copyright 2019 John Wiley and Sons. (G) An anti-counterfeiting PC pattern excited under different laser wavelengths.[278] Reproduced with permission from ref. 278, copyright 2018 Royal Society of Chemistry. (H) Multiresponsive elastic colloidal crystals for reversible structural-colour patterns.[279] Reproduced with permission from ref. 279, copyright 2019 John Wiley and Sons.

encryption relationship between optical stop-bands and information units. The hidden messages were protected by three different defence strategies: characteristic optical stop-bands, algorithm encryption and angle-dependent encryption, which could dramatically improve the security level of the hidden information. In combination with the large coding capacity, inherent optical stability and robust fabrication process, this PC coding system exhibited great potential for secure information storage (Fig. 18E).[89] Li *et al.* prepared a polymer film with moisture-responsive structural colour using the layer-by-layer assembly process. The film could reversibly hide/display high-resolution phone-shaped patterns at different humidity levels through the effect of membrane interference (Fig. 18F). The moisture response behaviour of the film could be selectively controlled by local UV-light crosslinking. This humidity-triggered colour change was fast, highly reversible, and compatible with most silicon-based devices (Fig. 18F).[277] Wang *et al.* showed a novel anti-forgery pattern by a combination of the "tricolour-fluorescence" property of carbon dots (CDs) and the unique microstructures constructed *via* a structured Si template or thermal treatment. Therefore, precisely assembled letter-shaped CD inverse opals (SiCDIOs) could be generated accordingly. The patterned SiCDIOs showed tricolour-fluorescence images when excited by laser light of 375, 480 and 560 nm. The signal was enhanced by a match between the fluorescence and the PC stopband (Fig. 18G).[278] Gu *et al.* fabricated a fruit-tree-shaped anti-counterfeiting pattern based on multiresponsive elastic colloidal crystals. Elastic poly(methyl methacrylate-butyl acrylate) copolymer nanoparticles with controlled sizes were fabricated through a one-step method and further served as building blocks for the construction of multiresponsive films *via* self-assembly. The combination of a low glass transition temperature and the core–shell structure of the copolymer nanoparticles made the material partially deform and fuse at room temperature under dry conditions, which eventually resulted in an enhancement of the mechanical properties as well as control over the optical properties. The generated elastic films could not only control concealment, for the exhibition of the designed colour information but also quickly respond to external stimuli such as the solvent, pH, and tensile force in a reversible fashion (Fig. 18H).[279]

4.4 Shape memory systems

Shape memory PCs, as a new research area that integrates scientific principles drawn from two disparate fields—PCs and shape memory materials—can temporarily assume a deformed microstructure and then revert to their original shape under an external stimulus; additionally, such a material exhibits optical bistability and thus provides a unique opportunity for constructing rewritable or reusable PCs.[35–39,290–294]

In this field, researches have mainly focused on the selection of shape memory polymers and on the external field stimulation of memory in PC systems.[37,38,290,291] Shape-memory generally includes programming, storage and recovery.[290] Here, programming involves deforming a bulk shape memory polymer from its permanent shape to a temporary configuration. This "hot" process is usually accomplished above a specific transition temperature, such as the polymer glass transition temperature, leveraging the compliant properties of a shape memory polymer against high temperatures. Once the sample is deformed, it is cooled to below the transition temperature for storage in the temporary shape. Recovery occurs when the sample is reheated to the vicinity of the transition temperature, which improves the polymer chain mobility and allows the shape memory polymer to return to its permanent shape *via* entropy elasticity.[290] The approaches to triggering the memory process of a shape memory PC are primarily from the action of heat, light, electromagnetic fields, *etc.*, and are basically realized either directly or indirectly through heat; that is, increasing the temperature of the polymer above its glass transition or melting point temperature causes the material to return to its original state. In recent years, a series of shape memory PC systems have been developed based on pressure memory and recovery by solvent immersion. For example, Jiang *et al.* developed arbitrary fingerprint and light-bulb PC patterns printed on new shape memory polymer membranes (Fig. 19A$_{ii}$); thus, a series of shape memory polymers capable of forming shapes *via* an unusual "cold" programming were obtained, and the shape recovery was triggered by applying a contact pressure under ambient conditions (Fig. 19A$_i$). Shape memory effects have been demonstrated at the nanoscale by combining fast-growing PC and shape memory polymer technologies. The fabrication of reconfigurable PCs has provided a simple and sensitive optical technique for intelligent system development (Fig. 19A).[290] Wang *et al.* presented the microscopic structure characteristics of shape memory poly(vinylidene fluoride-*co*-hexafluoropropylene) (PVDF-HFP) inverse opals together with those of bulk PVDF-HFP

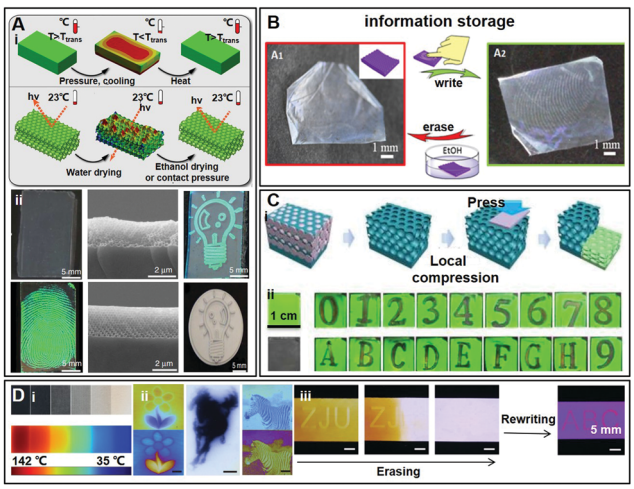

Fig. 19 (A) Reconfigurable PCs enabled by pressure-responsive shape memory polymers.[290] Reproduced with permission from ref. 290, copyright 2015 Springer Nature. (B) The concurrent microscopic structural characteristics for the shape memory effect of thermo-responsive PVDF-HFP inverse opals.[38] Reproduced with permission from ref. 38, copyright 2018 American Chemical Society. (C) Rewritable and highly stable PC patterns for optical storage and displays enabled by direct-pressure programmed shape memory PCs.[37] Reproduced with permission from ref. 37, copyright 2018 Royal Society of Chemistry. (D) Digital coding of mechanical stress in the dynamic and covalent network of a shape memory polymer.[291] Reproduced with permission from ref. 291, copyright 2018 Springer Nature.

by scanning electron microscopy. The materials showed a thermo-sensitive micro-SM property, accompanied by a reversible and modulated optical property. This feature was applied as a reversible write/erase record of fingerprint patterns activated *via* pressure stimulus and the solvent-induced effect, as demonstrated by the changes in the morphology/optical signal (Fig. 19B).[38] Zhang *et al.* presented rewritable and highly stable PC patterns acquired by polyethylene glycol diacrylate (PEGDA) and polyurethane acrylate (TAPU) copolymer shape memory PCs (Fig. 19C). The shape memory PCs presented a high-spatial resolution for potential applications in data storage and display panels based on the direct-pressure process. Because of the cross-linked polyurethane units and the reversible plastic strain at the nanoscale, the PEGDA-*co*-TAPU shape memory PCs exhibited high optical reversibility, excellent stability, and a direct pressure-induced programmability at room temperature (Fig. $19C_i$). Notably, multiple optical microarray patterns (numbers and letters) could be created by sequential imprinting. Shape memory PCs have provided a new optical platform for the fabrication of rewritable and high-stability PC patterns (Fig. $19C_{ii}$).[37] Recently, Xie *et al.* reported a digital photothermal mechanism based on laser printing and a thermally induced release that allowed for unparalleled freedom in the stress manipulation of the dynamic covalent network of a shape memory polymer without altering its shape (Fig. $19D_i$). Various arbitrary stress distributions were created in a free-standing polymer film utilizing a digital greyscale photothermal mechanism. The naturally invisible stresses could be further visualized as structural colours (such as flower, horse and letter pattern) under polarized light. The film was then restored to its original state *via* heating-induced release. This process has the potential for application in encoding hidden information (Fig. $19D_{ii,iii}$).[291]

5 Outlook and challenges

Inspired by the special functions of biological PC patterns, in this review, we summarize the recent research progress in the preparation strategies, functional evolution and applications of patterned PCs. A series of preparation strategies for PC patterns are described, including template-induced assembly and direct writing without a template. According to the functional evolution of this material, PC patterns can be divided into inactive and responsive PC patterns. The responsive PC patterns include reversible, immobilized and programmed PC patterns. Various applications of patterned PCs are also discussed in detail, for instance, sensors with a high sensitivity and fast response, PC displays based on external field regulation, information security *via* anti-counterfeiting devices and intelligent shape memory systems.

Although various PC patterns have been accomplished in recent years, there remain some challenges to the development of PC patterns as well as considerable room for material improvement. First, durability, compatibility, recyclability and large-scale fabrication of PC patterns are greatly required for real applications. Most of the PC patterns are disposable, high cost, or the substrates wear off severely after repeated use; these may be incompatible for real applications. Taking the anti-counterfeiting application of PC patterns in banknotes as an example, it should be checked whether the as-prepared pattern can be maintained after undergoing the whole manufacturing procedure of banknotes, or even whether the composite sample can withstand various testing conditions for real applications, such as multi-folding, solvent-resistance, wash-resistance, *etc.* In fact, many PC patterns have similar problems for further potential applications, there is a long way for overcoming the gap between the experimental samples to the real applications. Second, it is highly desirable to design and construct multi-functional PC patterns for advanced applications. The function of the currently prepared PC pattern is simple, resulting from the material response to only one or two stimuli. Therefore, designing, synthesizing, and introducing new type of molecule into PC systems are important for achieving advanced multi-functional applications of PC patterns.[215] Third, interdisciplinary research studies are required to develop the fabrication and applications of novel and advanced function PC patterns by chemistry, physics and materials science, engineering and biology. Learning from nature will provide great inspiration to create new PC patterns. Patterned colloidal PCs would bring about various novel optical devices with outstanding functions and widespread applications.

Conflicts of interest

There are no conflicts to declare.

Acknowledgements

We are grateful for the financial support from the National Key R&D Program of China (Grant No. 2016YFA0200803, 2017YFA0204504 and 2016YFB0402004), NSFC (Grant No. 51873221, 51673207 and 51373183), the Beijing Municipal Science & Technology Commission (Z181100004418012) and the Guangdong Provincial Key Laboratory of Optical Information Materials and Technology (2017B030301007).

Notes and references

1 Y. Y. Diao, X. Y. Liu, G. W. Toh, L. Shi and J. Zi, *Adv. Funct. Mater.*, 2013, **23**, 5373–5380.
2 D. Yang, S. Ye and J. Ge, *Adv. Funct. Mater.*, 2014, **24**, 3197–3205.
3 J. Hou, H. Zhang, Q. Yang, M. Li, L. Jiang and Y. Song, *Small*, 2015, **11**, 2738–2742.
4 M. Qin, Y. Huang, Y. Li, M. Su, B. Chen, H. Sun, P. Yong, C. Ye, F. Li and Y. Song, *Angew. Chem., Int. Ed.*, 2016, **55**, 6911–6914.
5 B. Zhu, Q. Fu, K. Chen and J. Ge, *Angew. Chem., Int. Ed.*, 2018, **57**, 252–256.
6 Z. Zhao, H. Wang, L. Shang, Y. Yu, F. Fu, Y. Zhao and Z. Gu, *Adv. Mater.*, 2017, **29**, 1704569.

7 D. Zhang, J. Liu, B. Chen, Y. Zhao, J. Wang, T. Ikeda and L. Jiang, *ACS Nano*, 2018, **12**, 12149–12158.
8 Z. Chen, F. Fu, Y. Yu, H. Wang, Y. Shang and Y. Zhao, *Adv. Mater.*, 2019, **31**, 1805431.
9 Y. Cao, L. Lewis, W. Y. Hamad and M. J. MacLachlan, *Adv. Mater.*, 2019, **31**, 1808186.
10 J. Hou, M. Li and Y. Song, *Nano Today*, 2018, **22**, 132–144.
11 Y. Shang, J. Wang, T. Ikeda and L. Jiang, *J. Mater. Chem. C*, 2019, **7**, 3413–3428.
12 L. Hu, Q. Zhang, X. Li and M. J. Serpe, *Mater. Horiz.*, 2019, **6**, 1774–1793.
13 B. Gao, L. Tang, D. Zhang, Z. Xie, E. Su, H. Liu and Z. Gu, *ACS Appl. Mater. Interfaces*, 2017, **9**, 32577–32582.
14 J. Hou, H. Zhang, Q. Yang, M. Li, Y. Song and L. Jiang, *Angew. Chem., Int. Ed.*, 2014, **53**, 5791–5795.
15 Y. Huang, F. Li, M. Qin, L. Jiang and Y. Song, *Angew. Chem., Int. Ed.*, 2013, **52**, 7296–7299.
16 L. Baldini, A. J. Wilson, J. Hong and A. D. Hamilton, *J. Am. Chem. Soc.*, 2004, **126**, 5656–5657.
17 M. Li, F. He, Q. Liao, J. Liu, L. Xu, L. Jiang, Y. Song, S. Wang and D. Zhu, *Angew. Chem., Int. Ed.*, 2008, **47**, 7258–7262.
18 K. Zhong, L. Wang, J. Li, S. V. Cleuvenbergen, C. Bartic, K. Song and K. Clays, *Langmuir*, 2017, **33**, 4840–4846.
19 P. Wu, J. Liu, Z. Xie, J. Guo and J. Wang, *Chin. J. Polym. Sci.*, 2018, **36**, 555–562.
20 L. Bai, V. C. Mai, Y. Lim, S. Hou, H. Mohwald and H. Duan, *Adv. Mater.*, 2018, **30**, 1705667.
21 M. Chen, Y. Tian, J. Zhang, R. Hong, L. Chen, S. Chen and D. Y. Son, *J. Mater. Chem. C*, 2016, **4**, 8765–8771.
22 D. Ge, E. Lee, L. Yang, Y. Cho, M. Li, D. S. Gianola and S. Yang, *Adv. Mater.*, 2015, **27**, 2489–2495.
23 S. Y. Lee, S.-H. Kim, H. Hwang, J. Y. Sim and S.-M. Yang, *Adv. Mater.*, 2014, **26**, 2391–2397.
24 Q. Li, Y. Zhang, L. Shi, H. Qiu, S. Zhang, N. Qi, J. Hu, W. Yuan, X. Zhang and K.-Q. Zhang, *ACS Nano*, 2018, **12**, 3095–3102.
25 C. Lin, Y. Jiang, C.-a. Tao, X. Yin, Y. Lan, C. Wang, S. Wang, X. Liu and G. Li, *ACS Appl. Mater. Interfaces*, 2017, **9**, 11770–11779.
26 S. Cho, T. S. Shim, J. H. Kim, D.-H. Kim and S.-H. Kim, *Adv. Mater.*, 2017, **29**, 1700256.
27 S. Y. Lee, J. Choi, J.-R. Jeong, J. H. Shin and S.-H. Kim, *Adv. Mater.*, 2017, **29**, 1605450.
28 H. Lee, T. Y. Jeon, S. Y. Lee, S. Y. Lee and S.-H. Kim, *Adv. Funct. Mater.*, 2018, **28**, 1706664.
29 X. Hu, Z. Huang, X. Zhou, P. Li, Y. Wang, Z. Huang, M. Su, W. Ren, F. Li, M. Li, Y. Chen and Y. Song, *Adv. Mater.*, 2017, **29**, 1703236.
30 Y. Zhan, Y. Wang, Q. Cheng, C. Li, K. Li, H. Li, J. Peng, B. Lu, Y. Wang, Y. Song, L. Jiang and M. Li, *Angew. Chem., Int. Ed.*, 2019, **58**, 1–8.
31 X. Du, M. Wang, A. Welle, F. Behboodi-Sadabad, Y. Wang, P. A. Levkin and Z. Gu, *Adv. Funct. Mater.*, 2018, **28**, 1803765.
32 Y. Heo, H. Kang, J.-S. Lee, Y.-K. Oh and S.-H. Kim, *Small*, 2016, **12**, 3819–3826.
33 H. Hu, J. Tang, H. Zhong, Z. Xi, C. Chen and Q. Chen, *Sci. Rep.*, 2013, **3**, 1484.
34 J. Hou, H. Zhang, B. Su, M. Li, Q. Yang, L. Jiang and Y. Song, *Chem. – Asian J.*, 2016, **11**, 2680–2685.
35 Y. Fang, S.-Y. Leo, Y. Ni, J. Wang, B. Wang, L. Yu, Z. Dong, Y. Dai, V. Basile, C. Taylor and P. Jiang, *ACS Appl. Mater. Interfaces*, 2017, **9**, 5457–5467.
36 S.-Y. Leo, W. Zhang, Y. Zhang, Y. Ni, H. Jiang, C. Jones, P. Jiang, V. Basile and C. Taylor, *Small*, 2018, **14**, 1703515.
37 W. Niu, K. Zhao, L. Qu and S. Zhang, *J. Mater. Chem. C*, 2018, **6**, 8385–8394.
38 M. Quan, B. Yang, J. Wang, H. Yu and X. Cao, *ACS Appl. Mater. Interfaces*, 2018, **10**, 4243–4249.
39 Y. Fang, Y. Ni, B. Choi, S.-Y. Leo, J. Gao, B. Ge, C. Taylor, V. Basile and P. Jiang, *Adv. Mater.*, 2015, **27**, 3696–3704.
40 F. Fu, Z. Chen, Z. Zhao, H. Wang, L. Shang, Z. Gu and Y. Zhao, *Proc. Natl. Acad. Sci. U. S. A.*, 2017, **10**, 1703616114.
41 Y. Zhang, Y. Wang, H. Wang, Y. Yu, Q. Zhong and Y. Zhao, *Small*, 2019, 1902198.
42 S. John, *Phys. Rev. Lett.*, 1987, **58**, 2486–2489.
43 E. Yablonovitch, *Phys. Rev. Lett.*, 1987, **58**, 2059–2062.
44 E. Yablonovitch, *J. Phys.: Condens. Matter*, 1993, **5**, 2443–2460.
45 Y. Zhao, Z. Xie, H. Gu, C. Zhu and Z. Gu, *Chem. Soc. Rev.*, 2012, **41**, 3297–3317.
46 M. Kuang, J. Wang and L. Jiang, *Chem. Soc. Rev.*, 2016, **45**, 6833–6854.
47 T. Guo, L. Heng, M. Wang, J. Wang and L. Jiang, *Adv. Mater.*, 2016, **28**, 8505–8510.
48 X. Gao, X. Yan, X. Yao, L. Xu, K. Zhang, J. Zhang, B. Yang and L. Jiang, *Adv. Mater.*, 2007, **19**, 2213–2217.
49 J. Huang, X. Wang and Z. L. Wang, *Nanotechnology*, 2008, **19**, 025602.
50 S. Vignolini, P. J. Rudall, A. V. Rowland, A. Reed, E. Moyroud, R. B. Faden, J. J. Baumberg, B. J. Glover and U. Steiner, *Proc. Natl. Acad. Sci. U. S. A.*, 2012, **109**, 15712–15715.
51 P. P. Goodwyn, Y. Maezono, N. Hosoda and K. Fujisaki, *Naturwissenschaften*, 2009, **96**, 781–787.
52 D. Gur, B. A. Palmer, B. Leshem, D. Oron, P. Fratzl, S. Weiner and L. Addadi, *Angew. Chem., Int. Ed.*, 2015, **54**, 12426–12430.
53 H. M. Whitney, M. Kolle, P. Andrew, L. Chittka, U. Steiner and B. J. Glover, *Science*, 2009, **323**, 130–133.
54 Y. Takeoka, *J. Mater. Chem.*, 2012, **22**, 23299–23309.
55 M. Wang, F. Meng, H. Wu and J. Wang, *Crystals*, 2016, **6**, 99.
56 J. Teyssier, S. V. Saenko, D. Marel and M. C. Milinkovitch, *Nat. Commun.*, 2015, **6**, 6368.
57 M. Vatankhah-Varnosfaderani, A. N. Keith, Y. Cong, H. Liang, M. Rosenthal, M. Sztucki, C. Clair, S. Magonov, D. A. Ivanov, A. V. Dobrynin and S. S. Sheiko, *Science*, 2018, **359**, 1509–1513.
58 G. H. Lee, T. M. Choi, B. Kim, S. H. Han, J. M. Lee and S.-H. Kim, *ACS Nano*, 2017, **11**, 11350–11357.
59 F. Liu, B. Q. Dong, X. H. Liu, Y. M. Zheng and J. Zi, *Opt. Express*, 2009, **17**, 16183–16191.
60 A. R. Parker and C. R. Lawrence, *Nature*, 2001, **414**, 33–34.
61 J. Zi, X. Yu, Y. Li, X. Hu, C. Xu, X. Wang, X. Liu and R. Fu, *Proc. Natl. Acad. Sci. U. S. A.*, 2003, **100**, 12576–12578.

62 Y. Zhao, X. Zhao and Z. Gu, *Adv. Funct. Mater.*, 2010, **20**, 2970–2988.
63 L. Shang, W. Zhang, K. Xu and Y. Zhao, *Mater. Horiz.*, 2019, **6**, 945–958.
64 J. B. Kim, S. Y. Lee, J. M. Lee and S.-H. Kim, *ACS Appl. Mater. Interfaces*, 2019, **11**, 14485–14509.
65 G. Isapour and M. Lattuada, *Adv. Mater.*, 2018, **30**, 1707069.
66 F. Fu, L. Shang, Z. Chen, Y. Yu and Y. Zhao, *Sci. Rob.*, 2018, **3**, eaar8580.
67 L. Bai, Z. Xie, W. Wang, C. Yuan, Y. Zhao, Z. Mu, Q. Zhong and Z. Gu, *ACS Nano*, 2014, **8**, 11094–11100.
68 Y. Wang, H. Cui, Q. Zhao and X. Du, *Matter*, 2019, **1**, 1–13.
69 Y. Liu, C. Shao, Y. Wang, L. Sun and Y. Zhao, *Matter*, 2019, **1**, 1–11.
70 T. Wang, S. R. Chen, F. Jin, J. H. Cai, L. Y. Cui, Y. M. Zheng, J. X. Wang, Y. L. Song and L. Jiang, *Chem. Commun.*, 2015, **51**, 1367–1370.
71 H. Kim, J. Ge, J. Kim, S. Choi, H. Lee, H. Lee, W. Park, Y. Yin and S. Kwon, *Nat. Photonics*, 2009, **3**, 534–540.
72 K. Chen, Q. Fu, S. Ye and J. Ge, *Adv. Funct. Mater.*, 2017, **27**, 1702825.
73 Y. Wang, D. Aurelio, W. Li, P. Tseng, Z. Zheng, M. Li, D. L. Kaplan, M. Liscidini and F. G. Omenetto, *Adv. Mater.*, 2017, **29**, 1702769.
74 P. Wu, J. Guo, K. Jiang, J. Wang and L. Jiang, *Adv. Funct. Mater.*, 2019, 1808473.
75 J. Liao, X. Li, Y. Wang, C. Zhang, J. Sun, C. Duan, Q. Chen and L. Peng, *Small*, 2012, **8**, 991–996.
76 S. M. Yang, H. Míguez and G. A. Ozin, *Adv. Funct. Mater.*, 2002, **12**, 425–431.
77 Z.-Z. Gu, A. Fujishima and O. Sato, *Angew. Chem., Int. Ed.*, 2002, **114**, 2171–2174.
78 D. Guo, X. Zheng, X. Wang, H. Li, K. Li, Z. Li and Y. Song, *Angew. Chem., Int. Ed.*, 2018, **57**, 16126–16130.
79 M. Gao, M. Kuang, L. Li, M. Liu, L. Wang and Y. Song, *Small*, 2018, **14**, 1800117.
80 B. Su, C. Zhang, S. Chen, X. Zhang, L. Chen, Y. Wu, Y. Nie, X. Kan, Y. Song and L. Jiang, *Adv. Mater.*, 2014, **26**, 2501–2507.
81 Y. Wang, C. Wei, H. Cong, Q. Yang, Y. Wu, B. Su, Y. Zhao, J. Wang and L. Jiang, *ACS Appl. Mater. Interfaces*, 2016, **8**, 4985–4993.
82 W. Fan, J. Zeng, Q. Gan, D. Ji, H. Song, W. Liu, L. Shi and L. Wu, *Sci. Adv.*, 2019, **5**, eaaw8755.
83 M. Zeng, D. King, D. Huang, C. Do, L. Wang, M. Chen, S. Lei, P. Lin, Y. Chen and Z. Cheng, *Proc. Natl. Acad. Sci. U. S. A.*, 2019, **116**, 18322–18327.
84 D. C. Hoekstra, K. Nickmans, J. Lub, M. G. Debije and A. Schenning, *ACS Appl. Mater. Interfaces*, 2019, **11**, 7423–7430.
85 M. Kuang, J. Wang, B. Bao, F. Li, L. Wang, L. Jiang and Y. Song, *Adv. Opt. Mater.*, 2014, **2**, 34–38.
86 L. Wu, Z. Dong, M. Kuang, Y. Li, F. Li, L. Jiang and Y. Song, *Adv. Funct. Mater.*, 2015, **25**, 2237–2242.
87 L. Cui, Y. Li, J. Wang, E. Tian, X. Zhang, Y. Zhang, Y. Song and L. Jiang, *J. Mater. Chem.*, 2009, **19**, 5499–5502.
88 S. Wu, B. Liu, X. Su and S. Zhang, *J. Phys. Chem. Lett.*, 2017, **8**, 2835–2841.
89 Y. Li, X. Zhou, Q. Yang, Y. Li, W. Li, H. Li, S. Chen, M. Li and Y. Song, *J. Mater. Chem. C*, 2017, **5**, 4621–4628.
90 P. Liu, J. Chen, Z. Zhang, Z. Xie, X. Du and Z. Gu, *Nanoscale*, 2018, **10**, 3673–3679.
91 J. Zhang, Z. Zhu, Z. Yu, L. Ling, C. Wang and S. Chen, *Mater. Horiz.*, 2019, **6**, 90–96.
92 X. He, Y. Gu, B. Yu, Z. Liu, K. Zhu, N. Wu, X. Zhao, Y. Wei, J. Zhou and Y. Song, *J. Mater. Chem. C*, 2019, **7**, 14069–14074.
93 G. H. Lee, J. Y. Sim and S.-H. Kim, *ACS Appl. Mater. Interfaces*, 2016, **8**, 12473–12480.
94 Z. Zhang, Z. Chen, L. Sun, X. Zhang and Y. Zhao, *Nano Res.*, 2019, **12**, 1579–1584.
95 Y. Zhang, P. Han, H. Zhou, N. Wu, Y. Wei, X. Yao, J. Zhou and Y. Song, *Adv. Funct. Mater.*, 2018, **28**, 1802585.
96 Y. Zhang, B. Dong, A. Chen, X. Liu, L. Shi and J. Zi, *Adv. Mater.*, 2015, **27**, 4719–4724.
97 Y. Ahn, E. Kim, J. Hyon, C. Kang and Y. Kang, *Adv. Mater.*, 2012, **24**, 127–130.
98 B. M. Boyle, T. A. French, R. M. Pearson, B. G. McCarthy and G. M. Miyake, *ACS Nano*, 2017, **11**, 3052–3058.
99 Y.-W. Chiang, J.-J. Chang, C.-Y. Chou, C.-S. Wu, E.-L. Lin and E. L. Thomas, *Adv. Opt. Mater.*, 2015, **3**, 1517–1523.
100 H. Eoh, H. S. Kang, M. J. Kim, M. Koo, T. H. Park, Y. Kim, H. Lim, D. Y. Ryu, E. Kim, J. Huh, Y. Kang and C. Park, *Adv. Funct. Mater.*, 2019, **29**, 1904055.
101 H.-F. Fei, W. Li, A. Bhardwaj, S. Nuguri, A. Ribbe and J. J. Watkins, *J. Am. Chem. Soc.*, 2019, **141**, 17006–17014.
102 H. S. Kang, J. Lee, S. M. Cho, T. H. Park, M. J. Kim, C. Park, S. W. Lee, K. L. Kim, D. Y. Ryu, J. Huh, E. L. Thomas and C. Park, *Adv. Mater.*, 2017, **29**, 1700084.
103 Y. Kang, J. J. Walish, T. Gorishnyy and E. L. Thomas, *Nat. Mater.*, 2007, **6**, 957–960.
104 A. L. Liberman-Martin, C. K. Chu and R. H. Grubbs, *Macromol. Rapid Commun.*, 2017, **38**, 1700058.
105 R. J. Macfarlane, B. Kim, B. Lee, R. A. Weitekamp, C. M. Bates, S. F. Lee, A. B. Chang, K. T. Delaney, G. H. Fredrickson, H. A. Atwater and R. H. Grubbs, *J. Am. Chem. Soc.*, 2014, **136**, 17374–17377.
106 G. M. Miyake, V. A. Piunova, R. A. Weitekamp and R. H. Grubbs, *Angew. Chem., Int. Ed.*, 2012, **51**, 11246–11248.
107 G. M. Miyake, R. A. Weitekamp, V. A. Piunova and R. H. Grubbs, *J. Am. Chem. Soc.*, 2012, **134**, 14249–14254.
108 T. J. Park, S. K. Hwang, S. Park, S. H. Cho, T. H. Park, B. Jeong, H. S. Kang, D. Y. Ryu, J. Huh, E. L. Thomas and C. Park, *ACS Nano*, 2015, **9**, 12158–12167.
109 V. A. Piunova, G. M. Miyake, C. S. Daeffler, R. A. Weitekamp and R. H. Grubbs, *J. Am. Chem. Soc.*, 2013, **135**, 15609–15616.
110 Y. Qiao, Y. Zhao, X. Yuan, Y. Zhao and L. Ren, *J. Mater. Sci.*, 2018, **53**, 16160–16168.
111 D.-P. Song, G. Jacucci, F. Dundar, A. Naik, H.-F. Fei, S. Vignolini and J. J. Watkins, *Macromolecules*, 2018, **51**, 2395–2400.
112 D.-P. Song, C. Li, N. S. Colella, X. Lu, J.-H. Lee and J. J. Watkins, *Adv. Opt. Mater.*, 2015, **3**, 1169–1175.
113 D.-P. Song, C. Li, W. Li and J. J. Watkins, *ACS Nano*, 2016, **10**, 1216–1223.

114 D.-P. Song, T. H. Zhao, G. Guidetti, S. Vignolini and R. M. Parker, *ACS Nano*, 2019, **13**, 1764–1771.
115 B. R. Sveinbjornsson, R. A. Weitekamp, G. M. Miyake, Y. Xia, H. A. Atwater and R. H. Grubbs, *Proc. Natl. Acad. Sci. U. S. A.*, 2012, **109**, 14332–14336.
116 D. Yamaguchi and T. Hashimoto, *Macromolecules*, 2001, **34**, 6495–6505.
117 Y. Yang, H. Kim, J. Xu, M.-S. Hwang, D. Tian, K. Wang, L. Zhang, Y. Liao, H.-G. Park, G.-R. Yi, X. Xie and J. Zhu, *Adv. Mater.*, 2018, **30**, 1707344.
118 Y.-G. Yu, C.-G. Chae, M.-J. Kim, H.-B. Seo, R. H. Grubbs and J.-S. Lee, *Macromolecules*, 2018, **51**, 447–455.
119 Y.-G. Yu, C. Seo, C.-G. Chae, H.-B. Seo, M.-J. Kim, Y. Kang and J.-S. Lee, *Macromolecules*, 2019, **52**, 4349–4358.
120 T. Zhang, J. Yang, X. Yu, Y. Li, X. Yuan, Y. Zhao, D. Lyu, Y. Men, K. Zhang and L. Ren, *Polym. Chem.*, 2019, **10**, 1519–1525.
121 Y. Yue, X. Li, T. Kurokawa, M. A. Haque and J. P. Gong, *J. Mater. Chem. B*, 2016, **4**, 4104–4109.
122 M. A. Haque, T. Kurokawa and J. P. Gong, *Soft Matter*, 2012, **8**, 8008–8016.
123 M. A. Haque, T. Kurokawa, G. Kamita, Y. Yue and J. P. Gong, *Chem. Mater.*, 2011, **23**, 5200–5207.
124 M. A. Haque, K. Mito, T. Kurokawa, T. Nakajima, T. Nonoyama, M. Ilyas and J. P. Gong, *ACS Omega*, 2018, **3**, 55–62.
125 Y. Yue and J. P. Gong, *J. Photochem. Photobiol., C*, 2015, **23**, 45–67.
126 Y. Yue, T. Kurokawa, M. A. Haque, T. Nakajima, T. Nonoyama, X. Li, I. Kajiwara and J. P. Gong, *Nat. Commun.*, 2014, **5**, 4659.
127 Y. F. Yue, M. A. Haque, T. Kurokawa, T. Nakajima and J. P. Gong, *Adv. Mater.*, 2013, **25**, 3106–3110.
128 C.-W. Chen, C.-C. Li, H.-C. Jau, L.-C. Yu, C.-L. Hong, D.-Y. Guo, C.-T. Wang and T.-H. Lin, *ACS Photonics*, 2015, **2**, 1524–1531.
129 W. He, G. Pan, Z. Yang, D. Zhao, G. Niu, W. Huang, X. Yuan, J. Guo, H. Cao and H. Yang, *Adv. Mater.*, 2009, **21**, 2050–2053.
130 M. Ravnik, G. P. Alexander, J. M. Yeomans and S. Zumer, *Proc. Natl. Acad. Sci. U. S. A.*, 2011, **108**, 5188–5192.
131 S. S. Lee, S. Kim, J. C. Won, Y. Kim and S.-H. Kim, *Angew. Chem., Int. Ed.*, 2015, **54**, 15266–15270.
132 S. S. Lee, J. B. Kim, Y. H. Kim and S.-H. Kim, *Sci. Adv.*, 2018, **4**, eaat8276.
133 S. S. Lee and S.-H. Kim, *Macromol. Res.*, 2018, **26**, 1054–1065.
134 L. Qin, J. Wei and Y. Yu, *Adv. Opt. Mater.*, 2019, **7**, 1900430.
135 J. Yang, J. Liu, B. Guan, W. He, Z. Yang, J. Wang, T. Ikeda and L. Jiang, *J. Mater. Chem. C*, 2019, **7**, 9460–9466.
136 J. Yang, W. Zhao, Z. Yang, W. He, J. Wang, T. Ikeda and L. Jiang, *J. Mater. Chem. C*, 2019, **7**, 13764–13769.
137 T. Wu, H. Li, J. Xue, X. Mo and Y. Xia, *Angew. Chem., Int. Ed.*, 2019, **58**, 1–7.
138 X. Sun, J. Zhang, X. Lu, X. Fang and H. Peng, *Angew. Chem., Int. Ed.*, 2015, **54**, 3630–3634.
139 C. G. Schäfer, M. Gallei, J. T. Zahn, J. Engelhardt, G. P. Hellmann and M. Rehahn, *Chem. Mater.*, 2013, **25**, 2309–2318.
140 S. Yang, N. Sun, B. B. Stogin, J. Wang, Y. Huang and T.-S. Wong, *Nat. Commun.*, 2017, **8**, 1285.
141 G. H. Lee, T. Y. Jeon, J. B. Kim, B. Lee, C.-S. Lee, S. Y. Lee and S.-H. Kim, *Chem. Mater.*, 2018, **30**, 3789–3797.
142 X. Jiang, H. Gao, X. Zhang, J. Pang, Y. Li, K. Li, Y. Wu, S. Li, J. Zhu, Y. Wei and L. Jiang, *Nat. Commun.*, 2018, **9**, 3799.
143 J. Feng, W. Wen, X. Wei, X. Jiang, M. Cao, X. Wang, X. Zhang, L. Jiang and Y. Wu, *Adv. Mater.*, 2019, **31**, 1807880.
144 X. Jiang, X. Zhang, Y. Wu, Y. Li, J. Pang, H. Zhang and L. Jiang, *Small*, 2019, **15**, 1900590.
145 Y. Yin, Y. Lu, B. Gates and Y. Xia, *J. Am. Chem. Soc.*, 2001, **123**, 8718–8729.
146 M. Rycenga, P. H. C. Camargo and Y. Xia, *Soft Matter*, 2009, **5**, 1129–1136.
147 S. Choi, I. Park, Z. Hao, H. N. Holman, A. P. Pisano and T. I. Zohdi, *Langmuir*, 2010, **26**, 4661–4667.
148 L. Mishchenko, B. Hatton, M. Kolle and J. Aizenberg, *Small*, 2012, **8**, 1904–1911.
149 Z. Xiao, A. Wang, J. Perumal and D.-P. Kim, *Adv. Funct. Mater.*, 2010, **20**, 1473–1479.
150 Y. Masuda, T. Itoh and K. Koumoto, *Langmuir*, 2005, **21**, 4478–4481.
151 X. Su, Y. Jiang, X. Sun, S. Wu, B. Tang, W. Niu and S. Zhang, *Nanoscale*, 2017, **9**, 17877–17883.
152 L. Shang, Y. Yu, W. Gao, Y. Wang, L. Qu, Z. Zhao, R. Chai and Y. Zhao, *Adv. Funct. Mater.*, 2018, **28**, 1705802.
153 Q. Wang, Z. Wang, Z. Li, J. Xiao, H. Shan, Z. Fang and L. Qi, *Sci. Adv.*, 2017, **3**, e1701183.
154 G. Wu, H. Cho, D. A. Wood, A. D. Dinsmore and S. Yang, *J. Am. Chem. Soc.*, 2017, **139**, 5095–5101.
155 J. Feng, X. Jiang, X. Yan, Y. Wu, B. Su, H. Fu, J. Yao and L. Jiang, *Adv. Mater.*, 2017, **29**, 1603652.
156 J. Feng, Q. Song, B. Zhang, Y. Wu, T. Wang and L. Jiang, *Adv. Mater.*, 2017, **29**, 1703143.
157 D. Guo, C. Li, Y. Wang, Y. Li and Y. Song, *Angew. Chem., Int. Ed.*, 2017, **56**, 15348–15352.
158 D. Guo, Y. Li, X. Zheng, F. Li, S. Chen, M. Li, Q. Yang, H. Li and Y. Song, *J. Am. Chem. Soc.*, 2018, **140**, 18–21.
159 B. Su, S. Wang, J. Ma, Y. Wu, X. Chen, Y. Song and L. Jiang, *Adv. Mater.*, 2012, **24**, 559–564.
160 Y. Wu, X. Chen, B. Su, Y. Song and L. Jiang, *Adv. Funct. Mater.*, 2012, **22**, 4569–4576.
161 Y. Wu, J. Feng, X. Jiang, Z. Zhang, X. Wang, B. Su and L. Jiang, *Nat. Commun.*, 2015, **6**, 6737.
162 B. Zhang, F. Meng, J. Feng, J. Wang, Y. Wu and L. Jiang, *Adv. Mater.*, 2018, **30**, 1707291.
163 T. Huang, Q. Zhao, J. Xiao and L. Qi, *ACS Nano*, 2010, **4**, 4707–4716.
164 Y. Yin and Y. Xia, *J. Am. Chem. Soc.*, 2003, **125**, 2048–2049.
165 Q. Li, Y.-W. Zhang, C.-F. Wang, D. A. Weitz and S. Chen, *Adv. Mater.*, 2018, **30**, 1803475.
166 S.-N. Yin, S. Yang, C.-F. Wang and S. Chen, *J. Am. Chem. Soc.*, 2016, **138**, 566–573.
167 X. Yang, D. Ge, G. Wu, Z. Liao and S. Yang, *ACS Appl. Mater. Interfaces*, 2016, **8**, 16289–16295.
168 D. Guo and Y. Song, *Chem. – Eur. J.*, 2018, **24**, 16196–16208.

169 Z. Huang, M. Su, Q. Yang, Z. Li, S. Chen, Y. Li, X. Zhou, F. Li and Y. Song, *Nat. Commun.*, 2017, **8**, 14110.
170 Z. Huang, Q. Yang, M. Su, Z. Li, X. Hu, Y. Li, Q. Pan, W. Ren, F. Li and Y. Song, *Adv. Mater.*, 2018, **30**, 1802172.
171 M. Su, Z. Huang, Y. Huang, S. Chen, X. Qian, W. Li, Y. Li, W. Pei, H. Chen, F. Li and Y. Song, *Adv. Mater.*, 2017, **29**, 1605223.
172 M. Su, Z. Huang, Y. Li, X. Qian, Z. Li, X. Hu, Q. Pan, F. Li, L. Li and Y. Song, *Adv. Mater.*, 2018, **30**, 1703963.
173 L. Wang, F. Li, M. Kuang, M. Gao, J. Wang, Y. Huang, L. Jiang and Y. Song, *Small*, 2015, **11**, 1900–1904.
174 M. Liu, J. Wang, M. He, L. Wang, F. Li, L. Jiang and Y. Song, *ACS Appl. Mater. Interfaces*, 2014, **6**, 13344–13348.
175 P. Kang, S. O. Ogunbo and D. Erickson, *Langmuir*, 2011, **27**, 9676–9680.
176 W. Li, Y. Wang, M. Li, L. P. Garbarini and F. G. Omenetto, *Adv. Mater.*, 2019, 1901036.
177 M. M. Moirangthem, A. F. Scheers and A. P. H. J. Schenning, *Chem. Commun.*, 2018, **54**, 4425–4428.
178 J. Wang, L. Wang, Y. Song and L. Jiang, *J. Mater. Chem. C*, 2013, **1**, 6048–6058.
179 Y.-L. Tong, Y.-W. Zhang, K. Ma, R. Cheng, F. Wang and S. Chen, *ACS Appl. Mater. Interfaces*, 2018, **10**, 31603–31609.
180 Z. Gu, Z. Huang, C. Li, M. Li and Y. Song, *Sci. Adv.*, 2018, **4**, eaat2390.
181 J. Sun, B. Cui, F. Chu, C. Yun, M. He, L. Li and Y. Song, *Nanomaterials*, 2018, **8**, 528.
182 Y. Huang, W. Li, M. Qin, H. Zhou, X. Zhang, F. Li and Y. Song, *Small*, 2017, **13**, 1503339.
183 X. Qian, Z. Cai, M. Su, F. Li, W. Fang, Y. Li, X. Zhou, Q. Li, X. Feng, W. Li, X. Hu, X. Wang, C. Pan and Y. Song, *Adv. Mater.*, 2018, **30**, 1800291.
184 Z. Gu, K. Wang, H. Li, M. Gao, L. Li, M. Kuang, Y. S. Zhao, M. Li and Y. Song, *Small*, 2017, **13**, 1603217.
185 Y. Huang, J. Zhou, B. Su, L. Shi, J. Wang, S. Chen, L. Wang, J. Zi, Y. Song and L. Jiang, *J. Am. Chem. Soc.*, 2012, **134**, 17053–17058.
186 Q. Yang, H. Li, M. Li, Y. Li, S. Chen, B. Bao and Y. Song, *ACS Appl. Mater. Interfaces*, 2017, **9**, 41521–41528.
187 L. Wang, J. Wang, Y. Huang, M. Liu, M. Kuang, Y. Li, L. Jiang and Y. Song, *J. Mater. Chem.*, 2012, **22**, 21405–21411.
188 Y. Li, M. Su, Z. Li, Z. Huang, F. Li, Q. Pan, W. Ren, X. Hu and Y. Song, *Small*, 2018, **14**, 1800792.
189 J. Park, J. Moon, H. Shin, D. Wang and M. Park, *J. Colloid Interface Sci.*, 2006, **298**, 713–719.
190 H. Ding, C. Zhu, L. Tian, C. Liu, G. Fu, L. Shang and Z. Gu, *ACS Appl. Mater. Interfaces*, 2017, **9**, 11933–11941.
191 Y. Li, Q. Yang, M. Li and Y. Song, *Sci. Rep.*, 2016, **6**, 24628.
192 S. Yu, X. Cao, W. Niu, S. Wu, W. Ma and S. Zhang, *ACS Appl. Mater. Interfaces*, 2019, **11**, 22777–22785.
193 J.-S. Lee, K. Je and S.-H. Kim, *Adv. Funct. Mater.*, 2016, **26**, 4587–4594.
194 X. Du, T. Li, L. Li, Z. Zhang and T. Wu, *J. Mater. Chem. C*, 2015, **3**, 3542–3546.
195 H. Fudouzi and Y. Xia, *Adv. Mater.*, 2003, **15**, 892–896.
196 D. P. Puzzo, A. C. Arsenault, I. Manners and G. A. Ozin, *Angew. Chem., Int. Ed.*, 2009, **48**, 943–947.
197 K. Zhong, J. Li, L. Liu, S. V. Cleuvenbergen, K. Song and K. Clays, *Adv. Mater.*, 2018, **30**, 1707246.
198 Y. Xie, Y. Meng, W. Wang, E. Zhang, J. Leng and Q. Pei, *Adv. Funct. Mater.*, 2018, **28**, 1802430.
199 H. Fudouzi and Y. Xia, *Langmuir*, 2003, **19**, 9653–9660.
200 Y. Hu, L. He and Y. Yin, *Angew. Chem., Int. Ed.*, 2011, **50**, 3747–3750.
201 J. Liu, L. Wan, M. Zhang, K. Jiang, K. Song, J. Wang, T. Ikeda and L. Jiang, *Adv. Funct. Mater.*, 2017, **27**, 1605221.
202 T. Tian, N. Gao, C. Gu, J. Li, H. Wang, Y. Lan, X. Yin and G. Li, *ACS Appl. Mater. Interfaces*, 2015, **7**, 19516–19525.
203 A. C. Arsenault, D. P. Puzzo, I. Manners and G. A. Ozin, *Nat. Photonics*, 2007, **1**, 468–472.
204 L. Nucara, F. Greco and V. Mattoli, *J. Mater. Chem. C*, 2015, **3**, 8449–8467.
205 T. S. Shim, S.-H. Kim, J. Y. Sim, J.-M. Lim and S.-M. Yang, *Adv. Mater.*, 2010, **22**, 4494–4498.
206 Y. Zhang, Y. Jiang, X. Wu and J. Ge, *J. Mater. Chem. C*, 2017, **5**, 9288–9295.
207 C. Zhu, W. Xu, L. Chen, W. Zhang, H. Xu and Z.-Z. Gu, *Adv. Funct. Mater.*, 2011, **21**, 2043–2048.
208 J. Ge, Y. Hu and Y. Yin, *Angew. Chem., Int. Ed.*, 2007, **119**, 7572–7575.
209 L. He, M. Wang, J. Ge and Y. Yin, *Acc. Chem. Res.*, 2012, **45**, 1431–1440.
210 M. Wang, L. He, W. Xu, X. Wang and Y. Yin, *Angew. Chem., Int. Ed.*, 2015, **54**, 7077–7081.
211 I. B. Burgess, L. Mishchenko, B. D. Hatton, M. Kolle, M. Loncar and J. Aizenberg, *J. Am. Chem. Soc.*, 2011, **133**, 12430–12432.
212 S. Yuan, W. Meng, A. Du, X. Cao, Y. Zhao, J. Wang and L. Jiang, *Chin. J. Polym. Sci.*, 2019, **37**, 729–736.
213 P. Chang, W. Niu, L. Qu and S. Zhang, *J. Mater. Chem. C*, 2019, **7**, 1896–1903.
214 S. Y. Lee, J.-S. Lee and S.-H. Kim, *Adv. Mater.*, 2019, 1901398.
215 M. M. Ito, A. H. Gibbons, D. Qin, D. Yamamoto, H. Jiang, D. Yamaguchi, K. Tanaka and E. Sivaniah, *Nature*, 2019, **570**, 363–367.
216 M. Vatankhah-Varnosfaderani, W. F. Daniel, M. H. Everhart, A. A. Pandya, H. Liang, K. Matyjaszewski, A. V. Dobrynin and S. S. Sheiko, *Nature*, 2017, **549**, 497–501.
217 Y. Zhang, L. Gao, L. Wen, L. Heng and Y. Song, *Phys. Chem. Chem. Phys.*, 2013, **15**, 11943–11949.
218 Y. Huang, F. Li, C. Ye, M. Qin, W. Ran and Y. Song, *Sci. Rep.*, 2015, **5**, 9724.
219 J. Huang, C.-a. Tao, Q. An, C. Lin, X. Li, D. Xu, Y. Wu, X. Li, D. Shen and G. Li, *Chem. Commun.*, 2010, **46**, 4103–4105.
220 R. Xuan, Q. Wu, Y. Yin and J. Ge, *J. Mater. Chem.*, 2011, **21**, 3672–3676.
221 M. Qin, F. Li, Y. Huang, W. Ran, D. Han and Y. Song, *Anal. Chem.*, 2015, **87**, 837–842.
222 W. Shen, M. Li, C. Ye, L. Jiang and Y. Song, *Lab Chip*, 2012, **12**, 3089–3095.
223 Z. Chen, M. Mo, F. Fu, L. Shang, H. Wang, C. Liu and Y. Zhao, *ACS Appl. Mater. Interfaces*, 2017, **9**, 38901–38907.

224 E. Tian, J. Wang, Y. Zheng, Y. Song, L. Jiang and D. Zhu, *J. Mater. Chem.*, 2008, **18**, 1116–1122.
225 L. Li, Y. Long, J.-M. Gao, K. Song and G. Yang, *Nanoscale*, 2016, **8**, 4458–4462.
226 I. B. Burgess, N. Koay, K. P. Raymond, M. Kolle, M. L. Lončar and J. Aizenberg, *ACS Nano*, 2012, **6**, 1427–1437.
227 X. Hong, Y. Peng, J. Bai, B. Ning, Y. Liu, Z. Zhou and Z. Gao, *Small*, 2014, **10**, 1308–1313.
228 Y. Zhang, Q. Fu and J. Ge, *Nat. Commun.*, 2015, **6**, 7510.
229 D. Yang, S. Ye and J. Ge, *J. Am. Chem. Soc.*, 2013, **135**, 18370–18376.
230 B. Yang, L. Li, K. Du, B. Fan, Y. Long and K. Song, *Chem. Commun.*, 2018, **54**, 3057–3060.
231 L. Duan, B. You, L. Wu and M. Chen, *J. Colloid Interface Sci.*, 2011, **353**, 163–168.
232 J. Chen, L. Xu, M. Yang, X. Chen, X. Chen and W. Hong, *Chem. Mater.*, 2019, **31**, 8918–8926.
233 D. Kou, W. Ma, S. Zhang, J. L. Lutkenhaus and B. Tang, *ACS Appl. Mater. Interfaces*, 2018, **10**, 41645–41654.
234 J. Yuan, X. Zhao, X. Wang and Z. Gu, *Sci. Rep.*, 2014, **4**, 6755.
235 X. Zhao, T. Ma, Z. Zeng, S. Zheng and Z. Gu, *Analyst*, 2016, **141**, 6549–6556.
236 N. Chang, J. Zhai, B. Liu, J. Zhou, Z. Zeng and X. Zhao, *Lab Chip*, 2018, **18**, 3638–3644.
237 B. Gao, A. Elbaz, Z. He, Z. Xie, H. Xu, S. Liu, E. Su, H. Liu and Z. Gu, *Adv. Mater. Technol.*, 2018, 1700308.
238 F. Zheng, Y. Cheng, J. Wang, J. Lu, B. Zhang, Y. Zhao and Z. Gu, *Adv. Mater.*, 2014, **26**, 7333–7338.
239 H. Wang, Z. Zhao, Y. Liu, C. Shao, F. Bian and Y. Zhao, *Sci. Adv.*, 2018, **4**, eaat2816.
240 J. MacLeod and F. Rosei, *Nat. Mater.*, 2013, **12**, 98–100.
241 Y. Xu, H. Wang, C. Luan, F. Fu, B. Chen, H. Liu and Y. Zhao, *Adv. Funct. Mater.*, 2018, **28**, 1704458.
242 Z. He, A. Elbaz, B. Gao, J. Zhang, E. Su and Z. Gu, *Adv. Healthcare Mater.*, 2018, 1701306.
243 M. Li, X. Lai, C. Li and Y. Song, *Mater. Today Nano*, 2019, **6**, 100039.
244 W. Luo, J. Yan, Y. Tan, H. Ma and J. Guan, *Nanoscale*, 2017, **9**, 9548–9555.
245 J. E. Stumpel, D. J. Broer and A. P. H. J. Schenning, *RSC Adv.*, 2015, **5**, 94650–94653.
246 Y. Qi, W. Niu, S. Zhang, S. Wu, L. Chu, W. Ma and B. Tang, *Adv. Funct. Mater.*, 2019, 1906799.
247 N. Ganesh, W. Zhang, P. C. Mathias, E. Chow, J. A. Soares, V. Malyarchuk, A. D. Smith and B. T. Cunningham, *Nat. Nanotechnol.*, 2007, **2**, 515–520.
248 X. Shi, L. Shi, M. Li, J. Hou, L. Chen, C. Ye, W. Shen, L. Jiang and Y. Song, *ACS Appl. Mater. Interfaces*, 2014, **6**, 6317–6321.
249 X. Shi, M. Li, C. Ye, W. Shen, Y. Wen, L. Chen, Q. Yang, L. Shi, L. Jiang and Y. Song, *Laser Photonics Rev.*, 2013, **7**, L39–L43.
250 D. Rout and R. Vijaya, *J. Appl. Phys.*, 2016, **119**, 023108.
251 F. Fu, L. Shang, F. Zheng, Z. Chen, H. Wang, J. Wang, Z. Gu and Y. Zhao, *ACS Appl. Mater. Interfaces*, 2016, **8**, 13840–13848.
252 E. Eftekhari, W. Wang, X. Li, N. A, Z. Wu, R. Klein, I. S. Cole and Q. Li, *Sens. Actuators, B*, 2017, **240**, 204–211.
253 S. Kedia and S. Sinha, *J. Phys. Chem. C*, 2015, **119**, 8924–8930.
254 L. Chen, X. Shi, M. Li, J. Hu, S. Sun, B. Su, Y. Wen, D. Han, L. Jiang and Y. Song, *Sci. Rep.*, 2015, **5**, 12965.
255 P. Shen, W. Li, Y. Liu, Z. Ding, Y. Deng, X. Zhu, Y. Jin, Y. Li, J. Li and T. Zheng, *Anal. Chem.*, 2017, **89**, 11862–11868.
256 X. Lu, H. Zhang, G. Fei, B. Yu, X. Tong, H. Xia and Y. Zhao, *Adv. Mater.*, 2018, **30**, 1706597.
257 S. Banisadr and J. Chen, *Sci. Rep.*, 2017, **7**, 17521.
258 W. Wei, Z. Zhang, J. Wei, X. Li and J. Guo, *Adv. Opt. Mater.*, 2018, **6**, 1800131.
259 J. Mu, G. Wang, H. Yan, H. Li, X. Wang, E. Gao, C. Hou, A. T. C. Pham, L. Wu, Q. Zhang, Y. Li, Z. Xu, Y. Guo, E. Reichmanis, H. Wang and M. Zhu, *Nat. Commun.*, 2018, **9**, 590.
260 T. Wu, J. Li, J. Li, S. Ye, J. Wei and J. Guo, *J. Mater. Chem. C*, 2016, **4**, 9687–9696.
261 H. Xing, J. Li, Y. Shi, J. Guo and J. Wei, *ACS Appl. Mater. Interfaces*, 2016, **8**, 9440–9445.
262 J. Liu, Y. Shang, D. Zhang, Z. Xie, R. Hu and J. Wang, *Chin. J. Polym. Sci.*, 2017, **35**, 1043–1050.
263 D. Zhang, J. Liu, B. Chen, J. Wang and L. Jiang, *Acta Chim. Sin.*, 2018, **76**, 425–435.
264 H. Wu, M. Kuang, L. Cui, D. Tian, M. Wang, G. Luan, J. Wang and L. Jiang, *Chem. Commun.*, 2016, **52**, 5924–5927.
265 J. Ge, J. Goebl, L. He, Z. Lu and Y. Yin, *Adv. Mater.*, 2009, **21**, 4259–4264.
266 X. Wu, R. Hong, J. Meng, R. Cheng, Z. Zhu, G. Wu, Q. Li, C.-F. Wang and S. Chen, *Angew. Chem., Int. Ed.*, 2019, **131**, 2–11.
267 G. Peng, Z. Zhu, Y. Tian, Y. Tong, T. Cui, C. Wang and S. Chen, *J. Mater. Chem. C*, 2018, **6**, 8187–8193.
268 Z. Yu, C.-F. Wang, L. Ling, L. Chen and S. Chen, *Angew. Chem., Int. Ed.*, 2012, **51**, 2375–2378.
269 J. Zhang, J. Liu, Z. Yu, S. Chen, O. A. Scherman and C. Abell, *Adv. Funct. Mater.*, 2018, **28**, 1800550.
270 H. Zhu, W. Fan, S. Zhou, M. Chen and L. Wu, *ACS Nano*, 2016, **10**, 9755–9761.
271 Z. Zhu, J. Zhang, C.-F. Wang and S. Chen, *Macromol. Mater. Eng.*, 2017, **302**, 1700013.
272 K. Liu, Y. Tian, Q. Li, X.-Y. Du, J. Zhang, C.-F. Wang and S. Chen, *J. Mater. Chem. C*, 2018, **6**, 2336–2341.
273 Y. Takeoka, S. Yoshioka, A. Takano, S. Arai, K. Nueangnoraj, H. Nishihara, M. Teshima, Y. Ohtsuka and T. Seki, *Angew. Chem., Int. Ed.*, 2013, **52**, 7261–7265.
274 H. S. Lee, T. S. Shim, H. Hwang, S.-M. Yang and S.-H. Kim, *Chem. Mater.*, 2013, **25**, 2684–2690.
275 Y. Liu, L. Shang, H. Wang, H. Zhang, M. Zou and Y. Zhao, *Mater. Horiz.*, 2018, **5**, 979–983.
276 Y. Qi, L. Chu, W. Niu, B. Tang, S. Wu, W. Ma and S. Zhang, *Adv. Funct. Mater.*, 2019, 1903743.
277 Z. Dong, N. Zhang, Y. Wang, J. Wu, Q. Gan and W. Li, *Adv. Funct. Mater.*, 2019, 1904453.
278 J. Liu, J. Ren, Z. Xie, B. Guan, J. Wang, T. Ikeda and L. Jiang, *Nanoscale*, 2018, **10**, 4642–4649.

279 J. Liao, C. Zhu, B. Gao, Z. Zhao, X. Liu, L. Tian, Y. Zeng, X. Zhou, Z. Xie and Z. Gu, *Adv. Funct. Mater.*, 2019, 1902954.
280 X. Chen, L. Wang, Y. Wen, Y. Zhang, J. Wang, Y. Song, L. Jiang and D. Zhu, *J. Mater. Chem.*, 2008, **18**, 2262–2267.
281 H. Nam, K. Song, D. Ha and T. Kim, *Sci. Rep.*, 2016, **6**, 30885.
282 M. Schaffner, G. England, M. Kolle, J. Aizenberg and N. Vogel, *Small*, 2015, **11**, 4334–4340.
283 R. Xuan and J. Ge, *Langmuir*, 2011, **27**, 5694–5699.
284 R. Xuan and J. Ge, *J. Mater. Chem.*, 2012, **22**, 367–372.
285 S. Ye, Q. Fu and J. Ge, *Adv. Funct. Mater.*, 2014, **24**, 6430–6438.
286 S. Ye and J. Ge, *J. Mater. Chem. C*, 2015, **3**, 8097–8103.
287 J. Zhang, S. Yang, Y. Tian, C.-F. Wang and S. Chen, *Chem. Commun.*, 2015, **51**, 10528–10531.
288 Y. Meng, F. Liu, M. M. Umair, B. Ju, S. Zhang and B. Tang, *Adv. Opt. Mater.*, 2018, **6**, 1701351.
289 C. Li, M. Zhao, X. Zhou, H. Li, Y. Wang, X. Hu, M. Li, L. Shi and Y. Song, *Adv. Opt. Mater.*, 2018, **6**, 1800651.
290 Y. Fang, Y. Ni, S.-Y. Leo, C. Taylor, V. Basile and P. Jiang, *Nat. Commun.*, 2015, **6**, 7416.
291 G. Zhang, W. Peng, J. Wu, Q. Zhao and T. Xie, *Nat. Commun.*, 2018, **9**, 4002.
292 Y. Fang, Y. Ni, S.-Y. Leo, B. Wang, V. Basile, C. Taylor and P. Jiang, *ACS Appl. Mater. Interfaces*, 2015, **7**, 23650–23659.
293 J. Wang, L. Sun, M. Zou, W. Gao, C. Liu, L. Shang, Z. Gu and Y. Zhao, *Sci. Adv.*, 2017, **3**, e1700004.
294 T. Xie, *Nature*, 2010, **464**, 267–270.